I.O.S.

SWANSEA BAY (SKER) PROJECT
TOPIC REPORT:7

R H WILKINSON

Foreshore sediment movement and its relation to observed tidal currents and wave climate

Report No 98

1980

NATURAL ENVIRONMENT RESEARCH COUNCIL

INSTITUTE OF OCEANOGRAPHIC SCIENCES

INSTITUTE OF OCEANOGRAPHIC SCIENCES

Wormley, Godalming,
Surrey, GU8 5UB.
(0428 - 79 - 4141)

(Director: Dr. A.S. Laughton)

Bidston Observatory,
Birkenhead,
Merseyside, L43 7RA.
(051 - 653 - 8633)

(Assistant Director: Dr. D.E. Cartwright)

Crossway,
Taunton,
Somerset, TA1 2DW.
(0823 - 86211)

(Assistant Director: M.J. Tucker)

SWANSEA BAY (SKER) PROJECT
TOPIC REPORT:7

R H WILKINSON

Foreshore sediment movement and its relation to observed tidal currents and wave climate

Report No 98

1980

This project is supported financially by
the Department of the Environment

Institute of Oceanographic Sciences
Crossway
Taunton
Somerset

June 1980

CONTENTS PAGE

1 INTRODUCTION

1.1 Preface

This report is the seventh in a series of Topic Reports resulting from a field investigation into the hydrodynamics, geology and thus the sedimentary regimes that exist in Swansea Bay. The purpose of this particular report is to describe the hydrodynamics of the nearshore zone, to evaluate the significance of longshore sediment transport on the eastern side of Swansea Bay and to attempt to relate the two. This assessment is based primarily on the results of two periods of experimental work in November 1976 and May 1977. During the experiments, the waves arriving at the beach tended to be smaller than the median monthly significant wave height experienced over the whole year, and no extremely severe conditions were experienced.

1.2 Geographical Considerations

The bay consists of a sedimentary coastline (mainly sandy) between two hard rock headlands at Mumbles and Porthcawl (Fig 1). It is often suggested (eg Komar (1976)) that such headlands form the boundaries to a littoral drift system, no sediment passing around them either into or out of the bay. Thus it may be possible to draw up a sediment budget inside this unit.

The four major rivers discharging into the bay are (clockwise) the Tawe, Neath, Afan and Kenfig. Stoner (1977) reported that 260 tonnes/day of suspended sediment are discharged into the bay, mainly by these rivers. This is interpreted by Collins et al (1979) as being silt sized sediment, and thus not contributing to the sand on the foreshore. The material on the eastern foreshore of the bay is fine to medium sized sand, as shown in Fig 5. However, there is only a surface layer of sand on the beach, which overlies peat and clay, which outcrop in several places. In many places, the layer of sand is so thin, that it can best be described as a 'veneer' (Blackley (1978)).

A prevalent idea in the literature is that a sedimentary coastline attempts to orient itself so that it becomes parallel to the predominant incoming wave crests (King (1972)). If these ideas are then associated with refraction and diffraction of water waves, the beach between the two hard rock headlands forms a 'crenulate' or 'logarithmic spiral' shaped bay (King (1972), Komar (1976), Silvester (1974), le Blond (1972) and many others). The resulting shoreline

and bathymetry in the bay is such that the wave crests, which are not originally parallel with the two 'anchoring' headlands, are refracted and diffracted until the wave breaks simultaneously and parallel to the shoreline. In this final condition, the wave-induced longshore drift of sediment (and water) is everywhere zero. Suitable local modifications must occur near the mouth of a river with any sort of sediment supply (eg the Neath) for the distribution of the alluvial sediment in a delta (see Komar (1976) Fig 10 - 12). The slope and orientation of Swansea Bay are very similar to those of a crenulate bay that would be the result of waves emanating from a south westerly direction.

1.3 Research Programme

The experiments reported here consisted of two periods of field work executed in November 1976 and May 1977, when simultaneous nearshore flow measurements were obtained whilst sand tracer studies were being performed. The flow measurements consisted of 3 components of velocity and the fluctuating pressure at a point 1 metre above the beach face recorded continuously when the instruments were submerged. The sediment transport was investigated by placing a known quantity of fluorescent sand tracer on the beach, and sampling at a grid of points on the beach over the next few tides in order to track any nett sand movement that might result from the action of the sea on the beach.

Additionally. other data of a more long-term nature, eg current meter records and wave climate studies, obtained during the course of the Swansea Bay (Sker) Project, has been consulted to extend the scope of the comments in this report.

Calculations are then made concerning the possible longshore sediment transport on the beach face using methods available in the literature, and the results of these calculations are compared with the experimental findings.

2 EXPERIMENTAL PROCEDURE AND ANALYSIS METHODS

Two series of field experiments were performed during which detailed measurements were made and the associated sediment movement on the beach was observed using fluorescent tracer techniques. The location selected for the study was midway between the southern breakwater of Port Talbot Tidal Harbour and Sker Point (see Fig 1(a)). This area of the beach was selected because it was covered uniformly by sand, unlike other regions of the beach which had clay and peat outcrops (Blackley (1978)). Also, it was anticipated that the proximity of the Tidal Harbour would have little or no effect. At this point, the beach had a cross section of uniform slope of 1 : 50, which is quite typical of the beach slopes along the eastern side of the Swansea Bay.

2.1 Flow Measurements

The nearshore flows were monitored using the instrument rig shown in Fig 2. The three components of velocity at a height of 1 m above the beach face were obtained using two orthogonally mounted electromagnetic flowmeters, each measuring two components of the flow with axes as shown. The orientation of the flowmeter heads and stems was checked with a levelling protractor after installation, and found to be satisfactory to within $\pm$ 1°. The fluctuating pressure at the same height that resulted from the passage of the waves was measured using an FM pressure transducer (Type NIO/4803). Also mounted on the rig can be seen a prototype instrument for the detection of sediment motion. The preamplifiers and the coil drive circuits for the electromagnetic flowmeters were installed in a watertight stainless steel can that was buried in the sand under the rig. This arrangement much improves the performance of the flowmeters when used with long cables. The rig holding these instruments was positioned 50m seaward of Ordnance Datum (OD), and hence the instruments themselves were in the horizontal plane of OD (Fig 3). Thus it was only possible for the instruments to be submerged over the top half of the tidal cycle. In fact, wave troughs below the mean water level dictate that they are really submerged for less than this time. As the beach slope is about 1 : 50, the height of the instruments above the beach (1m) results in them never being submerged less than 50m from the water's edge. To a first approximation, a wave breaks when it reaches water of depth equal to its height (Galvin (1972)), and so the instruments will not be inside the surf zone unless the waves are at least 1m high.

The other flow measurements referred to in this report are the tidal elevations at Port Talbot (kindly supplied by British Transport Docks Board) and the current meter records taken at Station K (see Fig 1) about 1km offshore from the experimental site. The tidal elevation was used as a measure of the mean depth of water over the instruments, as this varied with the state of the tide. The offshore current meter record was resolved into the components parallel to and perpendicular to the coast at that point.

The calibration curves used for the electromagnetic flowmeters were of the form $y = mx + c$, with the slopes being obtained in the laboratory by means of towing tank experiments, and these were assumed to take similar values in the field. It is well known that the offset 'c' is not constant between field and laboratory, and hence this must be found in situ. In this work, the zero offsets of the flowmeters were found by unfastening them from the rig at low tide and immersing the heads in a rubber bucket of sea water. It was thought that the output of the flowmeter electronics under these conditions would be equivalent to that given by a zero velocity of water passing the measuring head of the instrument. The pressure transducer was tested over the appropriate range of pressures in a calibration pressure vessel.

The four velocity signals from the electromagnetic flowmeters and the fluctuating pressure signal were recorded on an FM analogue tape recorder, whilst being monitored on a UV chart recorder. A flow diagram of these recording arrangements is given in Fig 4. The tidal elevation and offshore current meter records were continuous during most of the experiments, and so it was simply a matter of referring to the relevant part of these records.

An experimental run consisted of starting to record all the velocity and the pressure signals as soon as practicable after the instruments had been covered by the rising tide. Recording continued past high tide and on until the rig was nearly uncovered by the falling tide. The practicalities of ensuring that the instruments were not exposed by the wave troughs resulted in an experimental run being about 4 hours long.

2.2 Tracer Study of Sand Movement

During the periods when the velocities and pressures in the nearshore zone were being measured, attempts were made to estimate the resulting sediment motion on the beach face. This was done by placing a known quantity of fluorescent dyed sand (of similar hydraulic properties to the indigenous beach sand) near the instrumentation rig (see Fig 3) at low water. The

beach in the vicinity was then sampled over a grid of points at subsequent low tides. From the concentration of tracer found in the samples, a concentration distribution was obtained, and the position of the centroid of this distribution calculated. The movement of the centroid is then representative of the average movement of the sand particles in the region over which the samples are taken. The fundamental aspects of sediment tracer work, originally using radioactive tracers, can be found in Crickmore and Lean (1962) and details of and modifications to fluorescent tracer are given in Komar (1969).

The tracer used was a commercially dyed fluorescent sand ('Fesglow' - produced by British Industrial Sands). The grain size distribution as compared with the indigenous beach sand is given in Fig 5. Half tonne batches of the tracer were placed at the mid-tide level as shown in Fig 3. The method of injection was either by removing a 3.5m square of sand approximately 3cm thick from the beach and filling the hole with tracer, ending up flush with the existing beach, or placing the tracer in a low mound on the beach surface. Sometimes the tracer was wetted with a seawater/detergent mixture to eliminate surface tension or aeolian transport. The details of the tracer injections are given in Table 1.

The tracer was sampled at the nodes of a 50m x 50m grid that extended from high to low water and from 700m to the NW to 500m to the SE of the injection point in the longshore direction. Within the 50m square surrounding the injection site, the grid spacing was reduced to 12.5m x 12.5m. The sampling technique used for the coarse grid was to remove a 10cm x 10cm x 2cm deep portion of the beach face at the sample point using a specially designed scoop. Several 4cm diameter x 20cm deep cores were taken in the vicinity of the injection site to investigate the depth of movement. The limit of travel of the tracer along the beach was found wherever possible by examination of the exposed beach face at night under fluorescent light.

2.3 Analysis of Flow Measurements

The analogue magnetic tapes containing the 4 electromagnetic flowmeter records and the fluctuating pressure record were digitised at 5Hz after low pass filtering at 2.5Hz using techniques described by Davies et al (1977). An arbitrary record length of 10 minutes was chosen, which results in each record containing 3000 numbers. These files were then transferred to digital magnetic tape for subsequent analysis. The first step was to validate the data by producing time series plots for visual comparison with the field

UV chart records. Two major sources of error were apparent; spikes that were evident in the field records of the flowmeter outputs and digitisation errors that could occur in all channels. These anomalies were removed by manual editing.

The amplitude characteristics of the time series were examined by calculating the first four moments of the probability density function, ie the mean ($\bar{x}$), variance (σ_x^2), skewness (x_s) and kurtosis (x_k) respectively, in order to describe the shape of the distribution. The definitions used for the calculation of these quantities were :-

$$\bar{x} = \frac{1}{N} \sum_{i=1}^{N} x_i \qquad 2.1$$

$$\sigma_x^2 = \frac{1}{N} \sum_{i=1}^{N} (x_i - \bar{x})^2 \qquad 2.2$$

$$x_s = \frac{1}{N\sigma_x^3} \sum_{i=1}^{N} (x_i - \bar{x})^3 \qquad 2.3$$

$$x_k = \frac{1}{N\sigma_x^4} \sum_{i=1}^{N} (x_i - \bar{x})^4 \qquad 2.4$$

where x_i is the digitised version of the time series, and N is the number of values in a record (in this case $N = 3000$). This definition of kurtosis was used so that the kurtosis of a Gaussian distribution was zero.

The mean pressure, ie depth of water above the instruments, was not calculated from the above formula, but deduced from the tidal elevation record at Port Talbot, as the electronics of the pressure equipment was arranged to give an output equivalent to $(x_i - \bar{x})$.

Frequency analysis of the records was performed by calculating the Fourier sine and cosine coefficients corresponding to each data set using a Fast Fourier Transform computer subroutine. The coefficients could then be combined in the appropriate way to give autospectra of any desired time series or cross spectra between any two series. These techniques are standard and are reported by Rayment (1970), and more specifically for this work by Davies et al (1977) and Woodward (1978). The desired compromise between frequency resolution and confidence limits was reached by varying the number of estimates that were grouped together, keeping the record length constant at 10 minutes (ie 3000 digital values). Ensemble averaging was not relevant to the individual time series, as the seas were either decaying or not fully developed (Kinsman (1965)) and were not taken inside the breaker zone (Thornton (1979)), and so the 10 minute samples were never taken from a stationary random process.

2.4 Laboratory Analysis of Tracer Data

The coordinates of the centroid of the sediment tracer concentration distribution were found from:-

$$\bar{x} = \frac{\sum_{j=1}^{M} c_j x_j}{\sum_{j=1}^{M} c_j} \qquad 2.5$$

$$\bar{y} = \frac{\sum_{j=1}^{M} c_j y_j}{\sum_{j=1}^{M} c_j} \qquad 2.6$$

Where c_j is the concentration of the j^{th} sample in a total of M samples. The concentration was found by counting the number of grains (under fluorescent light) in a suitably sized well mixed aliquot of the sample, and so the units were grains/kg. If the centroid of the tracer distribution is obtained on two separate occasions, its movement is typical of the average sand grain in the search area (Crickmore and Lean (1962)). The longshore movement of

sand between the two searches was found from:-

$$Q_y = \Delta\bar{y} \times \Delta z' \times B \qquad 2.7$$

where $\Delta\bar{y}$ = change in longshore position of centroid

$\Delta z'$ = depth of movement

B = width of beach face/sampling zone

This is a volume movement; the mass of sand in motion is found by multiplying by the bulk density, and the rate of movement is obtained by dividing by the time between the sampling searches. Similarly the on/offshore movement of sand on the beach can be found.

It is important that the whole of the tracer cloud is taken into account, and that none has moved unknowingly out of the search area. As a check on how much tracer has been accounted for, the 'tracer budget' was examined, by comparing the amount of tracer detected with the quantity initially injected. The amount of tracer detected is:

$$Q_D = \sum_{i=1}^{M} c_i \left(\Delta x \Delta y \Delta z\right)_i \qquad 2.8$$

where $\Delta x\, \Delta y$ is the area of the grid square and Δz is the depth of sampling.

The quantity initially injected was found in two ways. Firstly, the number of grains could be calculated from the size frequency distribution and density of the tracer and the size of the injection. The second method was to physically count it, by making up a mixture of 1% tracer to 99% beach sand by weight and counting the number of tracer particles in a number of intimately mixed aliquots.

3 RESULTS AND DISCUSSION OF NEARSHORE FLOWS

3.1 Data Return

The data return for the November 1976 experiment was extremely poor. The pressure transducer functioned for most of the time and was successfully recorded, but the container in which the electromagnetic flowmeter electronics (ie pre-amplifier etc) were housed leaked, and so little velocity information

was obtained. Only three 1½ hour long complete data sets were recorded.

The success of the electronic flow measurements was much better during the repeated experiment in May 1977, when twelve experimental runs were performed, each of about 4 hours' duration. These were distributed over the whole range of tidal conditions, from neap to spring tides.

The vast majority of the following analysis has been performed using this May 1977 data, with a few checks on that from November 1976 where possible to confirm its similarity.

3.2 Amplitude Characteristics of Time Series

A typical five minute portion of the velocity and pressure records is shown in Fig 6. It can be seen that these are records of wave motion, as they show the typical 'groupiness' associated with surface water waves. The 'u' and the 'p' traces correspond visually to each other remarkably well. The 'u' trace that is reproduced here is that measured using head 2 (see Fig 2).

An example of the variation of the amplitude characteristics of these records over a complete experimental run (Run 12) is given in Fig 7. This run was recorded over a spring tide in May 1977. Examination of the mean, standard deviation, skewness and kurtosis curves reveals several factors, though these are not necessarily equally evident on each experimental run. One clear feature is that the shape of the probability density function is not completely defined by these four parameters. Examples of this are shown in Fig 8, where the probability density functions are shown for the time series of horizontal velocity measured by head 2 during run 12 starting at a) 0920 hours and b) 1210 hours. Distribution a) at first glance looks far more peaked (ie kurtosed) than does b) but the calculated kurtosis suggests otherwise.

The on/offshore velocity (u) was measured by two flowmeters with their heads oriented in different planes (see Fig 2). In Fig 7b, it can be seen that there is a difference between u_1 and u_2. The largest difference occurs (in this example) in the kurtosis, but the variance can differ by up to 15 - 20%. These discrepancies are largest when there is a large negative longshore velocity. Under these circumstances, the flow is approaching head 2 along the stem from the back of the head, possibly leaving the sensing electrodes in a region of stalled flow for some part of the wave cycle. This hypothesis is supported by probability density functions such as those shown in Fig 8. Data block 7M093 was obtained (at 0920 - 0930 hours) during

run 12, when the longshore velocity was -44 cms/sec, and data block 7M122 during the same run (at 1220 - 1230 hours) when the longshore velocity was +12 cms/sec. The large number of values near zero in the former (Fig 9a) correspond to the stalled flow condition. The reduced variance of u_2 compared with u_1 during these times is also consistent with this hypothesis. Consequently only the onshore velocity signals from head 1 are considered in the subsequent discussions.

The mean vertical velocities provide an insight into the accuracy of the zero offsets of the flowmeter signals. The procedure for determining the output of the instruments under zero velocity conditions was given in Section 2.1. Subsequent to these actions, an appreciable mean vertical velocity was often found. This remained approximately constant throughout an experimental run (see Fig 7b) but varied from run to run. It was too large to be accounted for by misalignment of the measuring head. If the waves had all been breaking in exactly the same position in relation to the instrumentation rig throughout the run, a non-zero mean vertical velocity could have been possible. However,'real' waves vary in height etc and so the break point for individual waves occur at different positions on the beach. Also, during a complete experimental run, the tide advances up the beach and back again. It is reasonable to assume that the incoming wave conditions remain fairly constant throughout a run, and so it can be considered that the velocity pattern due to the waves remains steady as it is convected past the head by the rising and falling tide. Thus, any long term mean (ie one taken over several hours) of the vertical velocity is an average both in time and space. Thus it was concluded that the non-zero mean vertical velocity, as evident in Fig 7b, was an artifact of the field calibration conditions. The act of placing the flowmeter measuring head in a rubber bucket of sea water by the side of the rig at low tide must have been different in some inconsistent way to true zero velocity conditions.

As all the electromagnetic flowmeter channels were constructed in the same way, there is no reason to suppose that the zero offsets of the u_1 or v_1 channels were any better behaved than that of the w_2 channel. Neither is there any reason to suggest that they behaved in an identical fashion, especially as these two channels were those measured by the other head. Thus it must be concluded that there is considerable uncertainty about the velocity zero on all channels, but one can be confident that any offset there is remains fairly constant during any particular run.

There are two changes to the oscillatory wave-induced velocities and pressures at the instrument position that might be expected to occur during a tidal cycle. It is assumed that the input wave conditions to the beach are constant throughout the period, and that the beach is of constant slope. The rising tide will have the effect of convecting a steady non-uniform wave field past the instruments, enabling comparative measurements to be made at different distances from the water's edge, and in different depths of water. Thus, at high tide, the breaker line is furthest from the instruments, and measurements taken at this time should show the least evidence of wave shoaling. That is, the onshore velocity and pressure traces should be more sinusoidal and symmetrical in the middle of an experimental run than those near the beginning or the end. Thus, as the tide rises, the skewness and kurtosis of the record should take values nearer to zero, indicating that the probability density function becomes more nearly Gaussian as the waves are measured further away from the break point.

Also, theoretical considerations indicated that the pressures and horizontal velocities measured in deeper water should be more highly attenuated, and hence for a given wave height, measurements of these quantities should have a smaller standard deviation if measured in deeper water. For example, the attenuation function for the subsurface pressure derived from first order linear wave theory is:

$$H(z) = \frac{\cosh k(h+z)}{\cosh kh} \qquad 3.1$$

where k = wave number of surface wave

h = water depth

z = vertical distance above bed

Evaluation of this expression for an 8 second period wave measured 1 m above the seabed shows that the $H(z)$ decreases from 95% to 86% (ie the attenuation increases) for a depth change from 2 to 5 m. Thus, if the wave conditions are constant, standard deviation of the velocity and pressure signals will be a function of depth. Therefore the standard deviation, skewness and kurtosis of the horizontal and pressure records should all vary with the state of the tide.

Neither of these trends was constantly visible (see for example, Fig 7). The standard deviation is not a normalised quantity, and hence is dependent on input wave height; a variation in the prevalent wave height of 10% will produce a change in the measured standard deviations of 10%. These quantities are also a function of the frequency content of the waves, as the attenuation is a function of their wavelength. Thus it is perhaps unrealistic to expect to see a tidal variation of the standard deviation which is only expected to be about 10%, unless the input waves are exceptionally constant.

Skewness and kurtosis should not be so sensitive to input conditions, as they are normalised quantities (see Eqns 2.1 to 2.4). However, the experimental results for these quantities also show little sign of a consistent pattern, the values of skewness and kurtosis tending to randomly fluctuate in the region of $\pm$ 0.5. When a wave shoals the onshore velocity becomes of a shorter duration, but is faster than the offshore velocity, ie the skewness of the velocity trace is positive. Similarly, the surface elevation spends less time above the mean water level than below it, but the crests are higher than the troughs are deep. The subsurface pressure should also follow this trend, and so be positively skewed. In fact, the examples shown in Fig 7 of pressure and onshore velocity do show a slight tendency for the skewness to be greatest at the ends of the experimental run when the water is at its most shallow, but this trend is not consistently shown for all runs.

As waves approach their breakpoint, especially on a shallow beach such as that at Sker where the breakers tend to 'spill', their shape changes from the smooth 'sinusoidal' type appearance to something like an asymmetrical saw tooth, with a short, steep front and a long flatter rear face. The probability density function of the former is Gaussian (the surface can be described as 'narrow band random noise'), and that of a saw tooth wave form is a 'boxcar' function, of length equal to the peak to peak fluctuation. Thus, as the wave shoals (ie measurements are taken nearer the breakpoint), it might be expected for the kurtosis to become negative, ie for the probability density function to become less peaked (ie 'platykurtic'). No sign of such a trend is visible in the results.

Very occasionally, the kurtosis departs from the region $\pm$ 0.5 and takes on a large, positive value, eg 5.27 and 5.96 in ω_k in Fig 7b.

Examination of the actual record showed that this was the result of the occasional large deviation from the mean. For instance, the value of 5.27 is the result of just one large fluctuation in the 10 minute run; it was thought that this was not real, but an instrumentation/digitisation error that had slipped through the data validation procedure.

However, a trend was visible in many of the mean longshore velocity results that correlated well with the tidal elevation. These two quantities are plotted as a Lissajous' figure in Fig 9. A definite pattern can be seen in this diagram, despite there being considerable scatter on both axes. The scatter in the velocity measurements appears between runs rather than during a run, and is thought to be a result of the uncertainty in the zero calibrations as explained previously. There will also be some uncertainty in the value of surface elevation, as this is taken from tidal records at Port Talbot 2 or 3 km from the experiment site. This is due to wave set down outside the breaker zone, which can be shown to be less than one quarter of the incident wave height (from the work of Bowen et al (1968)). The set down will be constant during a run, as the waves vary very little during this time. The agreement in Fig 9 is better for Spring tides when the flows are strongest. The circular/elliptical pattern (with axes parallel to those of the graph) indicate that the tidal wave is of a predominantly standing type in this region, as the velocity and tidal elevation are in quadrature. (The in phase components of a progressive wave would have produced a straight line.) This is in agreement with the Admiralty co-tidal chart of the area, which is reproduced from Heathershaw and Hammond (1980) in Fig 10. This shows that Swansea Bay is an area of nearly pure standing wave. Heathershaw and Hammond conclude that the phase of the longshore current is fairly constant along the whole length of the eastern shoreline, but the amplitude of the motion increases considerably from north west to south east, whilst being fairly constant perpendicular to the shore (fig 11 - also from Heathershaw and Hammond (1980)).

The invariance of the longshore current in a direction perpendicular to the shore is also shown in Fig 12. Here, the mean longshore component of the velocity from the electromagnetic flowmeter ($\bar{v}$) is plotted against the longshore component of the velocity (u_y) obtained from current meter (Fig 1). For most experimental runs (nine out of the twelve) $\bar{v}$ showed a very good one-to-one correspondence with u_y, especially away from

the ends of the runs (when the flowmeter might not be properly submerged). The mean slope of the lines of results for the nine runs was 0.94. The uncertain zero offset of $\bar{v}$ will introduce scatter in the form of a variable non-zero intercept on Fig 12. The electromagnetic flowmeter record only exists for times during which the instruments were submerged, ie over the top half of the tide. During this period, the distance of the flowmeter from the water's edge varied between 70 and 250m. The independence of the agreement between u_y and $\bar{v}$ from the distance from the water's edge suggests that the longshore velocity can be taken as constant from current meter K (which is about 1km offshore) to the seaward edge of the surf zone.

3.3 Frequency Analysis of Nearshore Flow Data.

The autospectra of the velocities and pressure measured at the beach rig were calculated and used to classify the size and type of waves arriving during the experiment. The wave conditions were fairly calm, the significant wave height varying from about 0.2 to 1m during the experiments, with an average over the month of May 1977 of 0.4m. The shapes of the spectra ranged from a single peak, typical of a swell sea (Fig 13(a)) to that more typical of a locally generated sea (Fig 13(b)), and any combination in between. There are various forms of equilibrium or saturation spectra proposed for surface water waves found either in the deep sea (Phillips (1958)) or in the breaker zone (Thornton (1979)). Comparison of the results with these is not justified, as the waves are neither fully developed nor breaking (Kinsman (1965)). The waves arriving at any particular time at the instrumentation rig are the sum of whatever storms and winds there happen to have been anywhere from the Bristol Channel to the mid-Atlantic and beyond and the resulting dissipation and refraction on the journey from source to beach.

However, comparison of simultaneously recorded autospectra with each other and examination of non-dimensional cross spectra (eg phase and coherency) can tell us absolute facts about the behaviour of the waves, and possibly waves in general, as long as the results are not too restricted in terms of wave height, etc.

The characteristics of wave records are usually examined by comparison with linear small amplitude (Airey) wave theory. To consider how closely the real waves under examination approximated to this ideal, the method of Simpson

(1969) was used. This is to calculate the empirical ratio between the energy in the horizontal velocity fluctuations and that in the pressure fluctuations (β_{emp}) and compare this, frequency (f) by frequency, with that predicted by linear theory (β_{TH}).

$$\beta_{emp} = \frac{S_{uu}(f) + S_{vv}(f)}{S_{pp}(f)} \qquad 3.2$$

$$\beta_{TH} = 4\pi^2 f^2 / g \tanh^2 kh \qquad 3.3$$

where $S_{uu}(f)$ = ordinate of 'u' autospectrum at frequency f etc

k = wave number of surface wave

h = water depth

Selected results for this comparison are shown in Fig 14. These were arbitrarily selected, and consisted of the 10 minute data block nearest high tide for all available runs, and one data block every $\frac{1}{2}$ hour for run 12. The results are classified by the depth of water in which they were obtained, with those obtained in a depth of between 1.5 and 2.5m being shown on the 'Depth = 2m' graph etc. The chain dotted curves are the upper and lower bounds of β_{TH} with the full curve for the middle of the depth range. The values of β_{emp} are shown as a dot for the ensemble average, with a scatter bar indicating the spread of results. There was no detectable difference in the characteristics of the results taken at high water from those taken anywhere else in the run. At high and low frequencies, β_{emp} is higher than the theoretical, indicating that there is more energy in the horizontal velocity of the motion compared with that in the pressure fluctuations than linear theory predicts. At low frequencies, this may be a result of slow fluctuations in the tidal longshore current ($\bar{v}$). This trend will also be accentuated by the fact that the pressure signal (for instrumental reasons) has a zero mean, and so $\beta_{emp}(f) \to \infty$ as $f \to 0$. At high frequencies, the excess velocity energy could be the result of turbulence generated by the waves themselves, or possibly by the longshore current. In fact, any high value of β_{emp} (apart from at very low frequencies) can be interpreted as being the result of turbulence, as any departure from Airy theory may be <u>defined</u> as turbulence (eg Seitz (1971) or Thornton (1979)). It may be that the waves are simply non-linear, but if this were the case, a significant amount of energy would appear

at harmonics of the fundamental wave frequency. This did not seem to be the case. It may have been better to consider this data in terms of the longshore bed shear stress (as an indicator of shear generated turbulence) instead of depth. However, at least a knowledge of the bedforms present would have been needed in addition to the mean velocity at a given height before any sort of bed shear stress estimate could have been made, and even then it was not considered that this estimate would have been very meaningful.

As the depth of water at the rig increases from 2m to 4m, the general agreement between theory and experiment improves. This is to be expected, as one of the small amplitude wave theory assumptions ($a \ll h$) is being more closely followed. There is, however, an inexplicable increase in the scatter when the depth increases to 5m.

An error in the calibration of either the flowmeter or pressure transducer would have the effect of raising or lowering the data by a consistent amount throughout the frequency range, as the behaviour of these instruments is linear in the region under consideration. The amount of scatter present in the results would conceal a certain amount of error of this type, but, for example, the 2m depth curves would require an error of the order of 100% to have been made, and this is most unlikely.

During some of the runs, the wave conditions were very gentle, and whereas this might be expected to give results more closely in accordance with small amplitude linear theory, the signal to noise ratio of the instrument/recording system must increase, and so introducing random scatter.

Thus the order of magnitude of the ratio between horizontal kinetic energy and pressure energy is satisfactorily predicted by linear theory, especially in water depths greater than 3m. In fact $\beta_{exp}(f)$ appeared to be independent of depth, even though the scatter was variable, and the improved agreement at the greater depths seemed to result from β_{TL} at those depths being more appropriate.

The horizontal velocity and pressure records were also compared by means of the squared coherency (γ^2) and phase spectra (Bendat and Piersol (1971)). This cannot be simply done unless the wave train is unidirectional (Yefimov

and Kristoforov (1971)), and so these comparisons were only made during records in which $\sigma_u \gg \sigma_v$. A typical example of u-p coherence is given in Fig 15. It was found that in most of, but not all, the experimental runs, if γ^2 was high, then the theoretical and empirical values of β agreed better (Fig 14) than if γ^2 was low. This is perhaps to be expected, for the fact that $\beta_{Emp} \approx \beta_{Th}$ means that (linear) Airey theory is a good approximation. Also, $\gamma^2 \approx 1$ indicates that u and p are behaving in a linearly related fashion. Thus, both γ^2 and β are indicators of linearity. In general, the u-p coherence was higher for records obtained during more vigorous wave conditions, which suggests that a poor signal to noise ratio of the instruments is a significant cause of low coherence.

Also shown in Fig 15 is the phase spectrum (ϕ) between u and p Linear theory shows that these two should be in phase with one another for a progressive wave. It can be seen that when $\gamma^2 \approx 1$ there is a tendency for p to lead u by a small angle of about 5°; when γ^2 is less than about 0.7, ϕ is too unreliable to interpret. Jenkins and Watts (1968) show that the confidence limits for ϕ with 10 degrees of freedom and $\gamma^2 > 0.9$ are better than $\pm 5^\circ$, and they reduce rapidly as $\gamma^2 \longrightarrow 1$. Thus the phase difference shown is probably real. The u-p coherence found in all the experimental runs, especially the one shown in Fig 15, is very high over all frequencies which contain a significant amount of energy, much higher than that found by Lukasik and Grosch (1963). The phase difference ϕ found here is also smaller than that found by these workers, but their confidence limits were wider.

One reason for out of phase behaviour of u and p is a departure from the purely progressive wave. The phase angle in a partial standing wave, which results from the addition of a partially reflected wave to the incident wave, can be written:

$$\tan \phi_{up} = \frac{2R}{(1-R^2)} \sin 2kx \qquad 3.4$$

where R is the amplitude reflection coefficient. When R is small (and thus ϕ is also small) this can be written for shallow water waves as:

$$\phi_{up} = 2R \sin\left\{\frac{4\pi f x}{\sqrt{gk}}\right\} \qquad 3.5$$

Thus if there is any reflected energy, it can be seen that ϕ_{up} takes on an oscillatory nature in the frequency (f) domain when measured at a given position (constant x). This is not apparent in the results where $\gamma^2 > 0.9$. Thus, as to be expected from such a gently sloping beach, there is no evidence of any reflected energy, and the phase shift must result from something else.

A reflected wave would also be apparent in the $u - \omega$ phase spectrum. Again, the addition of a partially reflected wave to the incident wave gives

$$\tan \phi_{u\omega} = \frac{R^2-1}{2R} \frac{1}{\sin 2kx} \qquad 3.6$$

Thus, when there is no reflection $(R=0)$, $\phi_{u\omega} = -90^\circ$ ie u and ω are in quadrature, with ω leading. The experimental results agree very well with this when $\gamma^2 = 1$, there being no reflection from the beach (see Fig 16). It is not uncommon for the coherency between u and ω to be poor for the following reasons. The vertical velocity under a surface wave tends to zero near the bed, and is small everywhere in a shallow water wave. Thus it is prone to poor signal to noise ratios, whether the source of the 'noise' is electronic or hydrodynamic, ie turbulence. All three components of shear generated turbulence are of about the same magnitude, and so the ω signal will be contaminated far more readily than the u signal by given turbulent conditions.

3.4 Directional Properties of Waves Approaching the Beach.

The angle of incidence of the waves just outside the surf zone is required for the calculation of wave induced longshore current velocities (Longuet-Higgins (1972)) and the estimation of wave-induced longshore drift of sediment (Komar and Inman (1970)) (See Appendices I and II). This angle can be estimated visually, but only with difficulty in the field, as the answer will be strongly biased towards the most visible frequency (which probably is that for which the waves are the steepest), rather than the most energetic.

The complete angular and frequency distribution of the wave energy is given by a directional spectrum (Longuet-Higgins et al (1963)). The measurements of u, v and p taken during these experiments were used to obtain the first five angular harmonics of this spectrum in the manner of Bowden and White (1966)

and Simpson (1969). The derivation of the theory is given by Simpson, and the programmes for combining the Fourier coefficients is described by Woodward (1978). This technique, which calculates the directional spectrum of the sea surface from measurements of the two horizontal velocity components and the pressure at a known point in the interior of the fluid, is dependent on small amplitude wave theory. Thus, unless all the inter-relationships between $\eta(t)$ (surface elevation), $u(t)$, $v(t)$ and $p(t)$ are at least linear, the answer will be inaccurate, just as one-dimensional calculations of $\eta(t)$ from $p(t)$ would be. Thus, unless the coherence between signals is good ($\gamma^2 \approx 1$ and $\beta_{TL} \approx \beta_{emp}$), the results must be treated with caution. The full directional spectrum of a given sea surface is a plot of the angular distribution of the energy in each frequency band. For theoretical reasons the angular spread of the energy is large (see Fig 17), and if there were waves of a similar frequency approaching from two directions, it would not be easy to differentiate between them. The usefulness of the full directional spectrum to beach work is further put into perspective when it is remembered that the direction of incident wave approach will be restricted to $\pm 60^\circ$ from the normal to the beach at the very most.

A more useful and compact result from the output of the directional spectrum computation is the graph of mean direction against frequency. For a unimodal narrow angular distribution, Cartwright (1963) shows this to be:

$$\tan \bar{\theta}(f) = C_{pv}(f) / C_{pu}(f) \qquad 3.7$$

where $C_{pv}(f)$ is the cross spectral estimate between $p(t)$ and $v(t)$ at frequency f etc. An example of this computation is given in Fig 18. Over the region for which γ^2_{pu} and γ^2_{uw} are about 1, it can be seen that the mean direction estimate is consistently near zero with very little scatter, ie the waves are normal to the beach. From records for which the coherency is less than 1, the large chaotic scatter extends over the whole frequency range. In Fig 18, this scatter is restricted to high and low frequencies, ie where $\gamma^2 < 1$

Fig 18 is typical of all the results in which confidence can be placed (ie those in which the waves are shown to be most linear). At the frequencies in which there is a significant amount of energy (between 0.1 and 0.3Hz) the mean incident wave direction was $0^\circ \pm 5^\circ$. Nothing more precise than this can be

said, as the confidence limits associated with the mean direction spectrum are unknown.

In shallow water, the U-V scatter plot may provide an alternative approach to obtaining an incident wave direction to the beach. Many scatter plots of this type were drawn (eg Fig 19) and an angle of wave approach was obtained by fitting a straight line to the data by minimisation of the sum of squares of the perpendiculars from the sample points to the line. In all the calculations performed, the angles obtained by this method agreed with the mean direction (averaged over frequencies of significant energy and coherence) obtained from the directional spectra, ie the waves were always normal to the beach to within 0.1°. The U-V scatter method will not detect reflection, and obviously is only relevant if $\sigma_u^2 \gg \sigma_v^2$ and the scatter plot is long and thin (similar to the narrow angular distribution limitation of Cartwright (1963)). The general statistical proof of this method has not been derived.

Estimates of a wave approach direction were also available from radar observations made from the end of the southerly breakwater at Port Talbot Tidal Harbour (Heathershaw et al (1980)). These were taken from October 1976 to November 1977 and the apparatus achieved a success rate of 50%. This resulted in data not being available during the periods of the beach experiments; however, the breakdowns were distributed throughout the year, and hence the results probably do give some indication of the angular wave climate. Of the waves that were detected by the use of radar, 75% were approaching in the sector between 230° and 240°, and 25% in that between 220° and 230°; the normal to the beach is at about 235°. These angular measurements are <u>not</u> related to the size of the waves. However, the limited wave approach angle for ocean, ie storm, waves can be seen by reference to the general orientation of the Bristol Channel (see Fig 1).

4 RESULTS OF TRACER EXPERIMENT AND DISCUSSION OF TECHNIQUES

The quantitative results from the tracer experiment were rather inconclusive. During the first experiment in November 1976, satisfactory tracer data were obtained, but unfortunately instrumentation failures led to a paucity of nearshore flow data for comparison. When the data from the May 1977 tracer experiments were examined, it became evident that the results were inextricably contaminated by tracer still present on the beach from the November experiment. Despite great effort, it proved impossible to calculate true tracer concentration distributions and longshore drift rates for the second experiment.

However, the fact that the tracer remained on the beach face for the entire

winter period is in itself evidence of the long term stability of the sand on the beach, reinforcing the geographical observations of Section 1.2. Fig 20 shows the longshore distribution of the blue tracer that was injected in November 1976 on gridline 10, as found by searches in May 1977, primarily intended to detect red tracer injected in the May experiment. The variance bars arise from both variability of tracer concentration across the beach section and variation between surveys. The across beach concentration profile is a maximum at the seaward edge (which is only 100m from the injection site, as these surveys were conducted on neap tides) gently decreasing to the top of the beach. The percentage recovery rate was 15%. It is most likely that the rest of the tracer has moved seawards, though the shape of the across beach concentration profile suggests that it has not gone far. The movement is possibly the result of the summer-winter variation in the beach profile (King (1972)). This shape of concentration profile would not result from landwards aeolian transport by the prevailing SW winds. The longshore concentration profile is very peaked when compared with the Gaussian distribution of similar longshore mean and radius of gyration (see Fig 20) and the centroid has only moved 46m in the 6 months since injection. This suggests both that the longshore diffusion processes are relatively inefficient and that the longshore advection of material is small. The tracer distribution is also remarkably compact when compared with the tidal excursion, which varies between 7km (neaps) and 14m (springs).

A typical contour plot of a tracer distribution found by one of the November beach surveys is shown in Fig 21. The position of the centroid of the tracer cloud with respect to an origin at the injection point was found from each search, and these are given in Table 2. The quantity of tracer accounted for by the tracer budget varied between 70% and 100% up to 10 days after injection which is higher than that normally achieved in this type of experiment (eg Komar (1969) reported a mean recovery rate of 56% during similar experiments). The main point of interest in the centroid movement results (Table 2) is the strong tendency for the initial movements of the tracer to be much larger than those on subsequent tides. After the initial high rate of movement, it appears as if the typical longshore centroid movement is of the order of 1m per tide, the direction being arbitrary.

It was thought that this behaviour was due to the tracer not being in equilibrium with the beach sand after injection, the tracer movement becoming slower and more representative of the beach sand movement as it becomes mixed with the indigenous sediment (similar to the offshore tracer studies of

Heathershaw and Carr (1978)). Several methods of injection were used (Section 2.2), but none was discernably better than the others. It is difficult to devise a field injection method that distributes the tracer vertically in the beach face down to the depth of disturbance. If the tracer is predominantly in the mobile topmost layers of the beach, a false impression of sand movement will result. It appears that the most satisfactory method is to allow the tracer to mix with the beach by natural processes, whatever they may be, and to take note of the results when the initial anomalous high rates of movement have subsided. During the experiment, an injection of tracer was followed up by searches on the next four low tides. However, it appears as if this is only just long enough for equilibrium conditions to be achieved, and future experiments should make provision for sampling over a longer period of time.

From practical considerations, the tracer was placed on the beach at mid-tide level in effectively a point injection when compared with the 400m wide beach face between low and high water spring tides. It was thought that the longshore movement of tracer from this point would be most representative of the movement of sand on the beach as a whole. However, Blackley and Carr (1977) show that the recorded variation in surface level on the beach is greatest at high and low water levels and least in the middle. Also, different parts of the beach are submerged, and thus subject to the action of the water, for different parts of the tidal cycle. It would be of interest to bear these points in mind in future experiments, and investigate possible variation in longshore movement across the beach section using several discrete injections of tracer along the section if a continuous injection is not practical.

5. MODEL OF LONGSHORE SAND TRANSPORT

Existing concepts of longshore drift of water and sediment along beaches tend to emphasise the role of waves approaching the beach obliquely (eg King (1972), Silvester (1974) and Komar (1976)). It has been suggested in this report (Section 1.2) that the shape of Swansea Bay as a whole is similar to that of a beach in long term equilibrium with the wave climate. It can be shown (Appendix 1) that the expected wave-induced longshore current velocities (which occur only in the immediate vicinity of the surf zone) are less than the measured longshore tidal current velocities, and that the latter extend inshore to the breaker line with little reduction (Section 3.2). The wave-induced longshore transport of sand is also restricted to the region of the surf zone, which is only of the order of 25m under normal conditions (Appendix 1). As the complete width of the beach face under consideration is about 400m, the effect

of the tidal longshore current could well be to transport much more material than the wave-induced longshore current. In this chapter, calculations are made to compare the relative competence of the wave-induced and tidal longshore currents.

5.1 Wave-Induced Littoral Drift

The wave-induced littoral drift of sediment was estimated by use of the concepts of 'longshore wave power' (Appendix 2). The formula, known sometimes as the 'CERC rating curve' was used to calculate the mass of quartz sand transported in half a tidal period (ie 6.4 hrs) in terms of the height (h) of the incoming waves, whose angle of incidence to the beach is θ_B

$$M_w = 6236\, h^{5/2} \sin 2\theta_B \text{ tonnes} \qquad 5.1$$

It is perhaps of interest to note the strong dependence of M_w on wave height 'h'. The wave-induced longshore current velocity in the surf zone is proportional to $\sqrt{h}$ (Appendix 1) and the cross-sectional area of the surf zone is proportional to h^2, hence the discharge of this littoral current goes as $h^{5/2}$, as does the mass flux of sediment. This may suggest that the mode of transport in the surf zone is suspended load, with a constant concentration of sand being convected by a larger amount of water. This finding is in contrast to Komar (1978) who argues that bed load is the predominant mode of transport in wave-induced littoral drift.

5.2 Tidally Induced Littoral Drift

The longshore tidal velocities recorded at the instrumentation rig (Section 3.2) achieve volumes of up to 1m/s, which is in excess of the threshold velocity for sand of the grain size found on this beach ($D_{35} \approx 0.15$mm, $U_{crit} \approx 0.2$ m/s - Shields (1936)). It can thus be expected that there will be some longshore movement of beach sand due to this tidal current. In order to calculate the order of magnitude of this littoral sand movement, the tidal currents and elevations were simplified to sinusoids (see Fig 22), the amplitudes and phases of which were taken from experiment (Section 3.2). The total load sediment transport rate Q_T was found using the Ackers and White formula (1973), modified to make allowance for the action of the waves by increasing the bed shear stress after the method of Bijker (1967). The calculations are fully described in Appendix 3. The calculation was performed for a number of tidal ranges representative of springs to neaps (10m to 5m) in the area and for a number of different wave heights at the beach. The results are shown in Fig 23

plotted as $\log M$ against $\log WHT$ where M is the mass moved in half a tide.

As expected, the tidally induced sediment transport is a function both of the tidal range and the wave height, but is much more strongly dependent on the former. For a beach of uniform slope, it can be deduced that Δx, the shoreward increment of the numerical integration, can be brought outside the summation, and is inversely proportional to the beach slope. Hence the mass of sand transported by the tide is also inversely proportional to the beach slope. Curves for three beach slopes are given in Fig 23.

5.3 Discussion

Fig 23 can now be used to estimate the relative sizes of the components of the sediment budget drawn up over a tidal cycle, bearing in mind that the beach at Morfa Mawr is of slope 1 : 50, and that the beach is oriented so that most of the very energetic waves arrive with a very small angle of incidence (Section 3.4). It can be seen that during spring tides, the tidal mechanism has far more longshore competence than any but the most exceptional waves, ie storm waves at an appreciable (and atypical, ie 5°) angle. During neap tides, tidal currents probably dominate the average wave conditions, but under storm conditions, waves would probably be the more effective agent.

It must be remembered that the tidal regime being discussed is a standing wave. The relation of the longshore currents to the state of the tide has been discussed (Appendix 3) and is summarised in Fig 24(a). For the standing wave, the tidal sediment transport over a tidal cycle is symmetrical, and thus no matter how big M_{TR}, it is equal and opposite to M_{TL}, the nett result being zero. Under the conditions of the experiments, $M_W \approx 0$, as the waves were always small, and were approaching normal to the beach anyway. However, in practical terms, it is very unlikely that M_{TR} is exactly equal to M_{TL}, and so it might be expected that small, random movements of the tracer centroid could result. This is exactly the type of behaviour observed after the tracer had had time to come into equilibrium with the beach sand.

The equivalent situation for a progressive tidal wave is shown in Fig 24(b). It can be seen that the top half of the beach is only exposed to currents in the direction of propagation of the tidal wave, and this could produce a nett longshore drift of material. The author is unaware of any evidence in the literature for this mechanism of longshore sediment drift.

The tidal current is not of equal amplitude all around Swansea Bay; they

nearly treble between Port Talbot Tidal Harbour and the southeast end of Morfa Mawr Beach. These horizontal gradients of velocity will result in horizontal gradients of sediment transport rate. At a point where the sediment transport rate is spatially increasing, there will be erosion, and when it is decreasing, there will be accretion. Thus, on a rising tide, this argument results in increasing erosion from the tidal harbour down towards Sker Point, and vice versa on the falling tide. It is possible that this increase in activity towards the SE could result in the increased long term variability in the beach profiles found by Blackley and Carr (1977).

To summarise this section, the local tidal currents are very capable of moving sediment along the beach - much more so than the prevailing wave climate. However, the standing nature of the tidal wave in this locality results in the nett amount moved in a complete tidal cycle being small; in fact it is theoretically zero.

6. CONCLUSIONS

During the experimental periods no evidence was found of either oblique wave approach to the beach or any wave-induced longshore current. Radar measurements of wave approach angle (Heathershaw et al (1980)) did not show a significant number of waves arriving at the beach at an oblique angle. Consideration of the compass bearing of significant fetches indicates that by far the greatest opportunities are for waves approaching the beach normally. The sediment tracer experiments revealed no preferential direction of sand movements in the short term (ie over one or two tidal cycles), or over the six months between the experiments.

The shape of Swansea Bay is similar to that of the crenulate bay. Such a bay is in a state of equilibrium with the prevailing wave climate, there having developed a certain bathymetry and shape of coastline which refracts and diffracts the waves so that they arrive normally to the local beach. In fact, refraction calculations show that all the ocean waves that arrive at the beach (8 secs period from the sector 220° to 270°) are refracted so that the local angle of incidence is small ($< \pm 3^{\circ}$).

The tide in this locality is a standing wave. The current resulting from the tidal wave extends with little reduction close inshore, nearly as far as the edge of the surf zone. Its magnitude is such that it is easily capable of mobilising a large amount of sediment, but its longshore action on the beach is symmetrical.

Thus the bay is in a long term equilibrium with the prevailing wave climate, and there is no predominant direction of sediment movement along the beach, in particular that on the Eastern coastline (Morfa Mawr). However, it must be remembered that the actual amount of sand present on the beach is very small (Blackley (1978)).

ACKNOWLEDGEMENTS

The author is grateful to Drs A P Carr and A D Heathershaw who organised and undertook the field experiments with the assistance of personnel from the electronics laboratory and M W L Blackley. Dr Carr and Mr Blackley performed the sediment tracer analyses. The author is also grateful to Mrs D J Corns for assistance with the data analysis and computing. The work was financially supported by the Department of the Environment.

REFERENCES

ACKERS, P and WHITE, W R 1973 Sediment transport - a new approach and analysis. Proceedings of the American Society of Civil Engineers, Journal of Hydraulics Division, 99, 2041 - 2060

BENDAT, J S and PIERSOL, A G 1971 Random data: analysis and measurement procedures. New York: John Wiley and Sons Inc, 407pp

BIJKER, E W 1967 The increse of bed shear in a current due to wave motion. pp746 - 765 in Proceedings 10th Coastal Engineering Conference Tokyo, 1966, 1. New York: American Society of Civil Engineers

BLACKLEY, M W L 1978 Swansea Bay (Sker) Project Topic Report 3. Geophysical interpretation and sediment characteristics of the offshore and foreshore areas. Institute of Oceanographic Sciences Report No 60 (unpublished manuscript), 42pp

BLACKLEY, M W L and CARR, A P 1977 Swansea Bay (Sker) Project Topic Report 2. Evidence for beach stability: photogrammetric and topographic measurements. Institute of Oceanographic Sciences Report No 51 (Unpublished manuscript), 45pp

LE BLOND, P H 1973 On the formation of spiral beaches. pp 1331 - 1345 in Proceedings 13th Coastal Engineering Conference, Vancouver, 1972, 2. New York: American Society of Civil Engineers

BOWDEN, K F and WHITE, R A 1966 Measurement of the orbital velocities of seawaves and their use in determining the directional spectrum. Geophysical Journal of the Royal Astronomical Society, 12, (1), 33-54

BOWEN, A J 1969 The generation of longshore currents on a plane beach. Journal of Marine Research, 27, (2), 206 - 215

BOWEN, A J, INMAN, D L and SIMMONS, V P 1968 Wave 'set down' and set up. Journal of Geophysical Research, 73, (8), 2569 - 2577

CARTWRIGHT, D E 1963 The use of directional spectra in studying the output of a wave recorder in a moving ship. pp 203 - 218 in Ocean Wave Spectra. Proceedings of a conference sponsored by the US Naval Oceanographic Office and the Division of Earth Science, National Academy of Sciences, National Research Council, Easton, Maryland USA 1961. Eaglewood Cliffs, New Jersey: Prentice-Hall Inc, 357pp

COLLINS, M, FERENTINOS,G and BANNER TF 1979 The hydrodynamics and sedimentology of a high (tidal and wave) energy embayment (Swansea Bay, Northern Bristol Channel). Estuarine and Coastal Marine Science, 8, (1), 49 - 74

CRICKMORE, M J and LEAN, G H 1962 The measurement of sand transport by means of radioactive tracers. Proceedings of the Royal Society of London, A, 266, (1326), 402 -421

DAVIES, A G, FREDERICKSEN,N F, and WILKINSON, R H 1977 The movement of non-cohesive sediment by surface water waves - Part II Experimental study. Institute of Oceanographic Sciences Report No 46 (unpublished manuscript), 54 pp

FORTNUM, B C H and HARDCASTLE, P J 1979 Waves recorded at Port Talbot on the South Wales coast. Institute of Oceanographic Sciences Report No 78 (unpublished manuscript), 8pp.

GALVIN, C J 1972 Wave breaking in shallow water. pp 413 - 456 in Waves on beaches and resulting sediment transport Proceedings of an advanced seminar conducted by the Mathematics Research Center University of Wisconsin and the Coastal Engineering Research Centre US Army at Madison, 1971. Edited by R E Meyer. New York: Academic Press, 462pp.

HEATHERSHAW, A D and CARR, A P 1978 Measurements of sediment transport rates using radioactive tracer pp 399 - 416 in Coastal Sediments '77 Proceedings of the 5th Symposium of the Waterway, Port, Coastal and Ocean Division of the American Society of Civil Engineers, Charleston, South Carolina 1977 New York: American Society of Civil Engineers, 1133 pp

HEATHERSHAW, A D and HAMMOND, F D C 1980 Swansea Bay (Sker) Project Topic Report: 4. Tidal currents: observed tidal and residual circulations and their response to meteorological conditions. Institute of Oceanographic Sciences, Report No 92 (unpublished manuscript), 154pp

HEATHERSHAW, A D, BLACKLEY, M W L, and HARDCASTLE, P H 1980 Wave direction in coastal waters using radar. Coastal Engineering, 3, 249-267.

JENKINS, G M and WATTS, D G 1968 Spectral analysis and its applications. San Francisco: Holden-Day, 525pp

KING, C A M 1972 Beaches and Coasts. London: Edward Arnold, 570pp

KINSMAN, B 1965 Wind Waves. Eaglewood Cliffs, New Jersey: Prentice-Hall Inc, 676 pp.

KOMAR, P D 1969 The longshore transport of sand on beaches. University of California, San Diego, Ph D Thesis, 143 pp

KOMAR, P D 1976 Beach processes and sedimentation. Eaglewood Cliffs New Jersey: Prentice Hall Inc, 429 pp

KOMAR, P D 1978 Relative quantities of suspension versus bed-load transport on beaches. Journal of Sedimentary Petrology, 48, (3), 921-932

KOMAR, P D and INMAN, D L 1970 Longshore sand transport on beaches. Journal of Geophysical Research, 75, (30), 5914 - 5927

LONGUET-HIGGINS, M S 1952 On the statistical distribution of the heights of sea waves. Journal of Marine Research, 11, (3), 245 - 266

LONGUET-HIGGINS, M S 1973 The mechanics of the surf zone. pp 213 - 228 in Applied Mechanics, Proceedings of 13th International Congress of Theoretical and Applied Mechanics, Moscow 1972. Edited by E Becker and G K Mikhailov. Berlin: Springer-Verlag.

LONGUET-HIGGINS, M S, CARTWRIGHT, D E and SMITH, N D 1963 Observations of the directional spectrum of sea waves using the motions of a floating buoy. pp 111 - 131 in Ocean Wave Spectra. Proceedings of a conference sponsored by the US Naval Oceanographic Office and the Division of Earth Sciences, National Academy of Sciences National Research Council, Easton, Maryland, USA, 1961. Eaglewood Cliffs, New Jersey: Prentice-Hall Inc, 357 pp.

LUKASIK, S J and GROSCH, C E 1963 Pressure and velocity correlations in ocean swell. Journal of Geophysical Research, 68, (20), 5689 - 5699

RAYMENT, R 1970 Introduction to the First Fourier Transform (FFT) in the production of spectra. Meteorological Magazine, 99, (1178), 261 - 269

SEITZ, R C 1971 Measurement of a three-dimensional field of water velocities at a depth of 1 m in an estuary. Journal of Marine Research, 22, (2), 140 - 150

SHIELDS, A 1936. Application of similarity principles and turbulence research to bed load movement. Mitteilungen der Preussischen Versuchanstalt für Wasserbau und Schiffbau, Berlin (translation in California Institute of Technology Hydrodynamics Laboratory Publication No 167)

SILVESTER, R 1974 Coastal Engineering 2. Amsterdam: Elsevier Scientific Publishing Company, 338 pp.

SIMPSON, J H 1969. Observations of the directional characteristics of sea waves. Geophysical Journal of the Royal Astronomical Society, 17, (1), 93 - 120

STONER, J H 1977. A report on the first year of a programme to monitor inputs to Swansea Bay 1973/74. Welsh National Water Development Authority Report, No 55 TW 77/2, 24 pp

THORNTON, E B 1979 Energetics of breaking waves within the surf zone. Journal of Geophysical Research, 84, (C8), 4931 - 4938

WOODWARD, B W 1978 Wave direction characteristics in the nearshore zone. Institute of Oceanographic Sciences (Taunton) Industrial Placement Report (unpublished manuscript), 75 pp

YEFIMOV, V V and KRISTOFOROV, G N 1971 Spectra and statistical relations between the velocity fluctuations in the upper layer of the sea and surface waves. Izvestya Atmospheric and Oceanic Physics, 7, (12), 1290 - 1310

Time and date of injection	Colour of tracer	Area of injection site (m^2)	Thickness of injection (cms)	Notes
0530 hrs 14/11/76	Red	12.5	2.8	Placed in shallow excavation in beach. Neap tides.
0030 hrs 22/11/76	Blue	12.5	2.8	Placed in shallow excavation in beach. Spring tides.
0030 hrs 22/11/76	Yellowy-green	6.3	5.5	Shallow mound on beach surface (immediately N of above). Spring tides.
0540 hrs 26/4/77	Red	12.5	2.8	Placed in shallow excavation in beach. Neap tides.
1500 hrs 2/5/77	Blue	25.0	1.4	Placed just N of previous sites as red tracer still near surface at injection site. Spring tides.

All injections consisted of 0.5 tonnes of tracer

TABLE 1 Details of Fluorescent Tracer Injections.

Search Number	Number of Tides since injection	$\bar{y}$ (m)	$\bar{x}$ (m)	$\Delta\bar{y}$/tide	$\Delta\bar{x}$/tide
Red Tracer					
1	1	18.06	22.45	18.06	22.45
2	2	52.04	8.61	33.98	-13.84
3	3	52.09	-3.06	-0.05	-11.67
4	4	49.08	-0.81	-3.01	2.25
5	16	73.91	50.55	1.95	4.28
6	17	73.22	39.58	-0.69	-10.97
7	18	77.84	42.90	4.62	3.32
8	19	59.66	39.93	-18.18	-2.97
Blue Tracer					
5	1	-1.04	25.74	-1.04	25.74
6	2	0.68	0.28	0.68	0.28
7	3	1.40	0.51	1.40	0.51
8	4	0.61	6.83	0.61	6.83
Green Tracer					
5	1	-2.61	27.25	-2.61	27.25
6	2	-0.51	26.44	2.10	-0.81
7	3	-0.24	26.84	0.27	0.40
8	4	0.09	27.52	0.33	0.68

TABLE 2 Detail of Tracer Centroid Movement (Nov. 1970)

APPENDIX 1

WAVE-INDUCED LONGSHORE CURRENTS

These currents occur only in the vicinity of the surf zone, and as no measurements were taken in this region, the velocities and their distribution must be deduced from theoretical arguments. The radiation stress theories of wave-induced longshore currents (eg Longuet-Higgins (1972); Bowen (1969)) are now accepted to be the best explanation of the generation of these currents. The radiation stress is the excess horizontal momentum flux caused by the passage of surface water waves, and it is the onshore flux of longshore momentum by a train of waves at an oblique angle to the coast that is the relevant component in this context. There is a change in momentum flux when energy is dissipated from the waves, and hence by far the greatest change occurs in the breaker zone, where the rate of dissipation is greatest. It is this change in momentum flux that produces the driving force for the longshore currents.

Longuet-Higgins (1972) showed that the wave-induced longshore current had a triangular velocity distribution (see Fig 25) with the maximum being:

$$V_B = \frac{5\pi}{8} \frac{\alpha S}{C} \sqrt{g l_B} \sin \theta_B \qquad 1A.1$$

The following assumptions were made:

(i) Complete dissipation of energy on the beach (no reflection)

(ii) Breaker height is a fixed proportion ($2\alpha \approx 0.8$) of the water depth (l_B).

(iii) Linear wave theory holds in the surf zone to the first order.

(iv) Chézy (quadratic) friction law is appropriate for evaluation of bottom stress (C = Chézy coefficient).

(v) Beach slope is constant (= S).

(vi) Waves are at a small angle of incidence (θ_B).

(vii) No lateral (horizontal) mixing.

The fact that a real wave train is polychromatic and contains waves of many heights means that it breaks at a variable distance from the shore. This, together with lateral mixing, modifies the profile to that shown dotted.

Longuet-Higgins recommends the use of values of 0.4 and 0.01 for α and C respectively, and hence on a beach of slope S = 1 : 50 (as at the experimental site):

$$V_B = 7.8\sqrt{a_B}\,\sin\theta_B \qquad \text{1A.2}$$

where $2a_B$ is the height of the wave at the breakpoint. The median of the monthly significant wave heights measured at Port Talbot by Fortnum and Hardcastle (1979a) was 0.5m, giving an RMS value of 0.35m (Longuet-Higgins, (1952)). It has been shown that angles of wave incidence greater than $\pm 5^\circ$ would be most unusual, and so using Equation 1A.2, it can be seen that wave-induced velocities in the surf zone will be generally much less than 0.3m/s.

This current is restricted to the surf zone. As waves break when their height $\approx$ water depth (Galvin (1972)), the width of the surf zone is of the order:

$$x_B \approx 2a_B/S \qquad \text{1A.3}$$

At the site of the experiment (where $S \approx 1/50$) a wave height of 0.5m results in a surf zone 25m wide. The wave statistics of Fortnum and Hardcastle suggest that this is not unusual.

APPENDIX 2

ESTIMATION OF WAVE-INDUCED LONGSHORE DRIFT OF SEDIMENT

For many years, a relationship has been developed between longshore transport of sediment and 'longshore wave power'. After many years of empirical correlation, Longuet-Higgins (1972) and Komar and Inman (1970) developed a theoretical derivation for the then favoured form of the formula, which is sometimes known as the 'CERC rating curve'. The theoretical derivation and dimensional considerations show that the term 'longshore wave power' is misleading, if not incorrect, and that the relevant quantity is 'onshore flux of longshore momentum', ie it is another radiation stress argument. In its most detailed form, Komar and Inman suggest:

$$I_l = k' \left(EC_n\right)_B \cos\theta_B \frac{\langle v_l \rangle}{u_m} \qquad 2A.1$$

where I_l = immersed weight transport rate in entire surf zone

$(EC_n)_B$ = wave energy flux evaluated at breaker line

θ_B = angle of incidence of waves at breaker line

u_m = wave orbital velocity

and $\langle v_l \rangle$ = longshore current of unspecified origin.

It must be emphasised that this is the <u>total</u> wave-induced transport, ie both bed load and suspended load summed across the surf zone. If $\langle v_l \rangle$ is the result of waves alone,

$$I_l = K \left(EC_n\right)_B \sin\theta_B \cos\theta_B \qquad 2A.2$$

where $K = 0.77$ (empirical)

Taking $\left(EC_n\right)_B = \frac{1}{2} \rho g^{3/2} a^{5/2} \alpha^{-1/2}$ (Longuet-Higgins (1970)) 2A.3

then $I_l = 9.35 \times 10^{3} a^{5/2} \sin 2\theta_B \qquad 2A.4$

If the wave amplitude 'a' is measured in metres, then the units of I_l are newtons/sec. It is more convenient if this is written as a mass flux:

$$Q_w = \frac{\rho_s}{(\rho_s - \rho)g} I_l \qquad 2A.5$$

ie $$Q_w = 1531\, a^{5/2} \sin 2\theta_B \quad \text{Kg/sec} \qquad \text{2A.6}$$

For comparison with the tidally induced transport, the mass moved in half a tide (ie 6.4hrs) by the wave-induced littoral drift is:

$$M_w = 6236\, a^{5/2} \sin 2\theta_B \quad \text{tonnes} \qquad \text{2A.7}$$

APPENDIX 3

ESTIMATION OF TIDALLY INDUCED LONGSHORE DRIFT OF SEDIMENT

The empirical evidence given in Section 3.2 shows that the longshore tidal currents behave very much like a standing wave, and so can be written as:

$$\eta(t) = -\frac{TR}{2}\cos\omega t \qquad 3A.1$$

$$V_{100}(t) = \frac{TR}{20}\sin\omega t \qquad 3A.2$$

where $\eta(t)$ is the tidal elevation, TR is the tidal range and $V_{100}(t)$ is the longshore tidal current 1m above the sea bed (Fig 22). The relationship between the amplitude of $\eta(t)$ and $V_{100}(t)$ is empirical, and they are assumed to be constant across the beach section.

The standing nature of the tidal wave means that, starting at low water, the current sweeps the beach in a positive direction (ie NW-SE) as the tide rises, being zero at high and low water and maximum at mid-tide. The reverse happens on a falling tide, and so the action of the tidal currents on the beach is symmetrical, the nett effect being zero. In order to assess the sediment transporting capacity of the tidal stream, the amount of sand moved in half a tidal cycle is examined. It is hypothesised that a mass M_{TR} is transported in a positive direction by the rising tide, and an equal mass M_{TL} is moved in a negative direction by the falling tide. The sediment budget over the tidal cycle will appear thus:

$$\Sigma M = M_{TR} - M_{TL} + 2M_W \qquad 3A.3$$

The mass of sand transported to the right by the rising tide was calculated from:

$$M_{TR} = \int_{\text{Low tide}}^{\text{High tide}} \int_{\text{Low water}}^{\text{Water's edge}} Q_T \, dx \, dt \qquad 3A.4$$

$$\approx \sum_{N=1}^{20} \left\{ \Delta t_N \sum_{i=1}^{N} Q_{T_i} \Delta x \right\} \qquad 3A.5$$

The integral was evaluated numerically by replacing the smooth tidal elevation curve by 20 equal depth increases as shown in Fig 22. The total load sediment transport rate Q_T was found using the Ackers and White formula (1973). As it is expected that the incoming waves will 'feel bottom' over the whole width of the beach face, the bottom stress used in the Ackers and White method (deduced from logarithmic velocity distribution assumptions) must be modified to account for the action of the waves. This was done by increasing the bottom stress by a factor evaluated by the method of Bijker (1967); the use of this combination for longshore sediment movement calculations was evaluated by Swart (1976) and found to be the most satisfactory available. It results in the transport rate being written as:

$$Q_T = Q_T \left(V_{HT}, HT, z_0, depth, D_{35}, W_{HT}, \lambda \right)$$

where
- V_{HT} = longshore current at height HT above the bed
- z_0 = bed roughness ($\sim$ 0.5cm)
- $depth$ = depth of flow
- D_{35} = 35 percentile grain size diameter (0.15mm)

} defines log velocity profile and hence bed shear stress.

- W_{HT} = wave height
- λ = wave length

} Used to calculate wave orbital velocity and hence Bijker stress magnification factor

All parameters for calculating Q_T were taken as the time average over the variable time interval. The calculation was performed for a number of tidal ranges representative of spring to neap tides in the area (10m to 5m) and for a number of different wave heights. The results are shown in Fig 23.

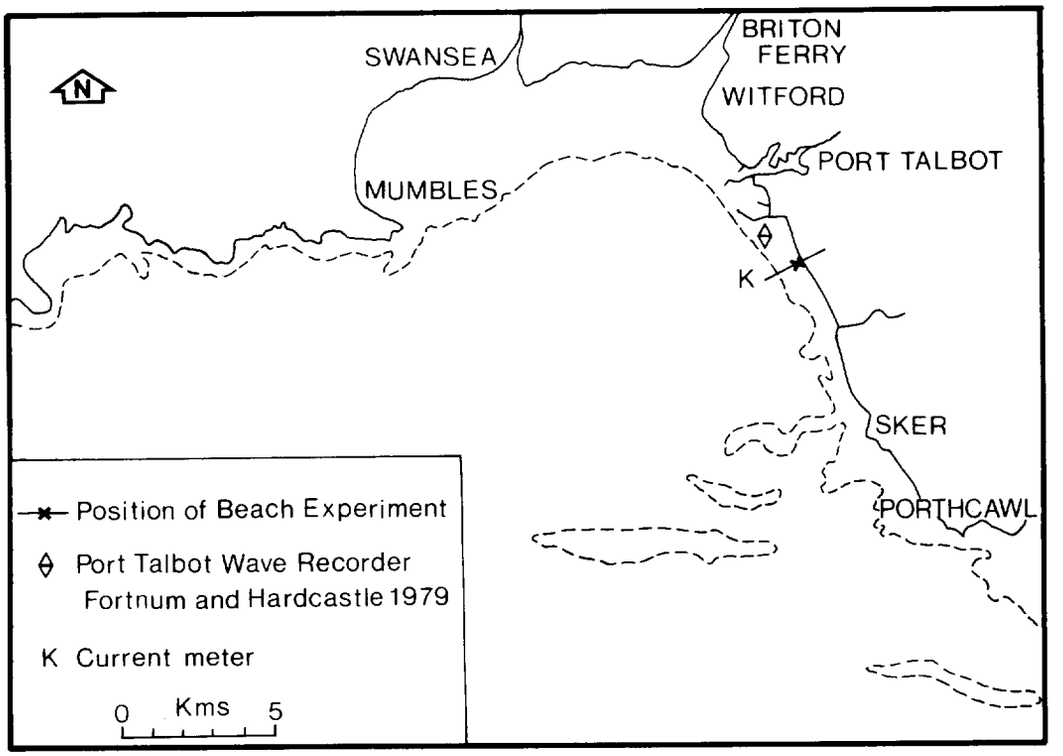

Fig 1. Geographical location of Swansea Bay and experimental site

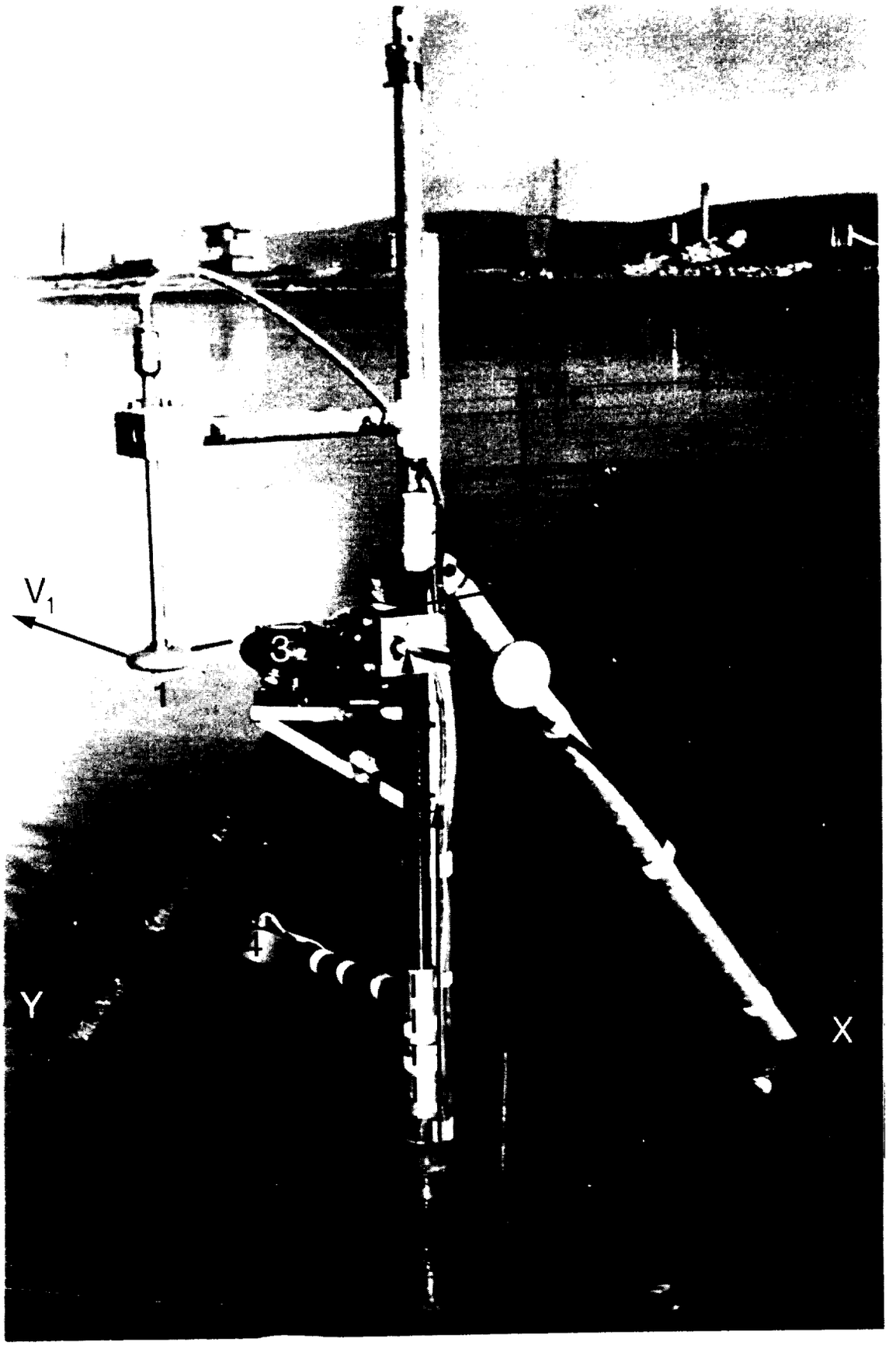

Fig 2. Instrumentation rig with coordinate axes

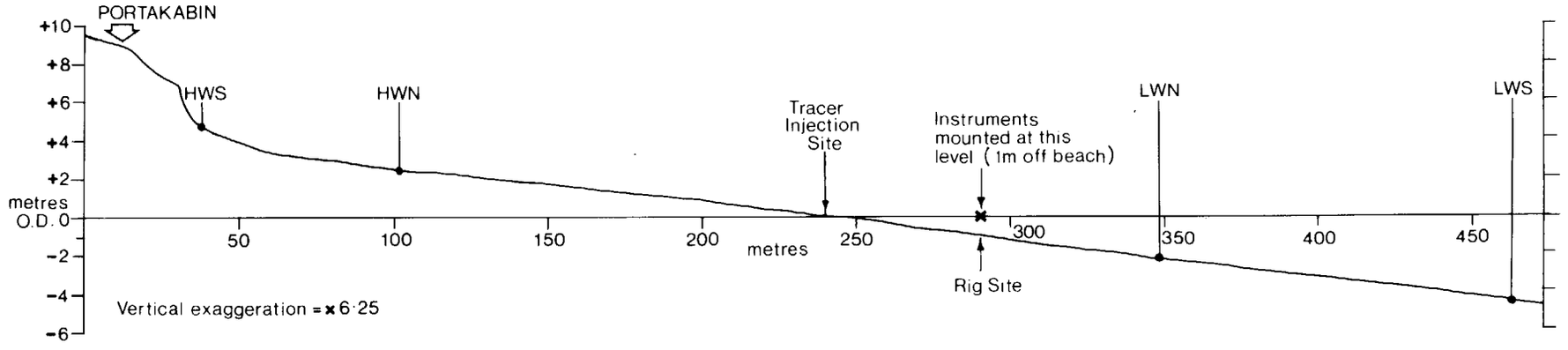

Fig 3. Position of instruments on beach cross-section

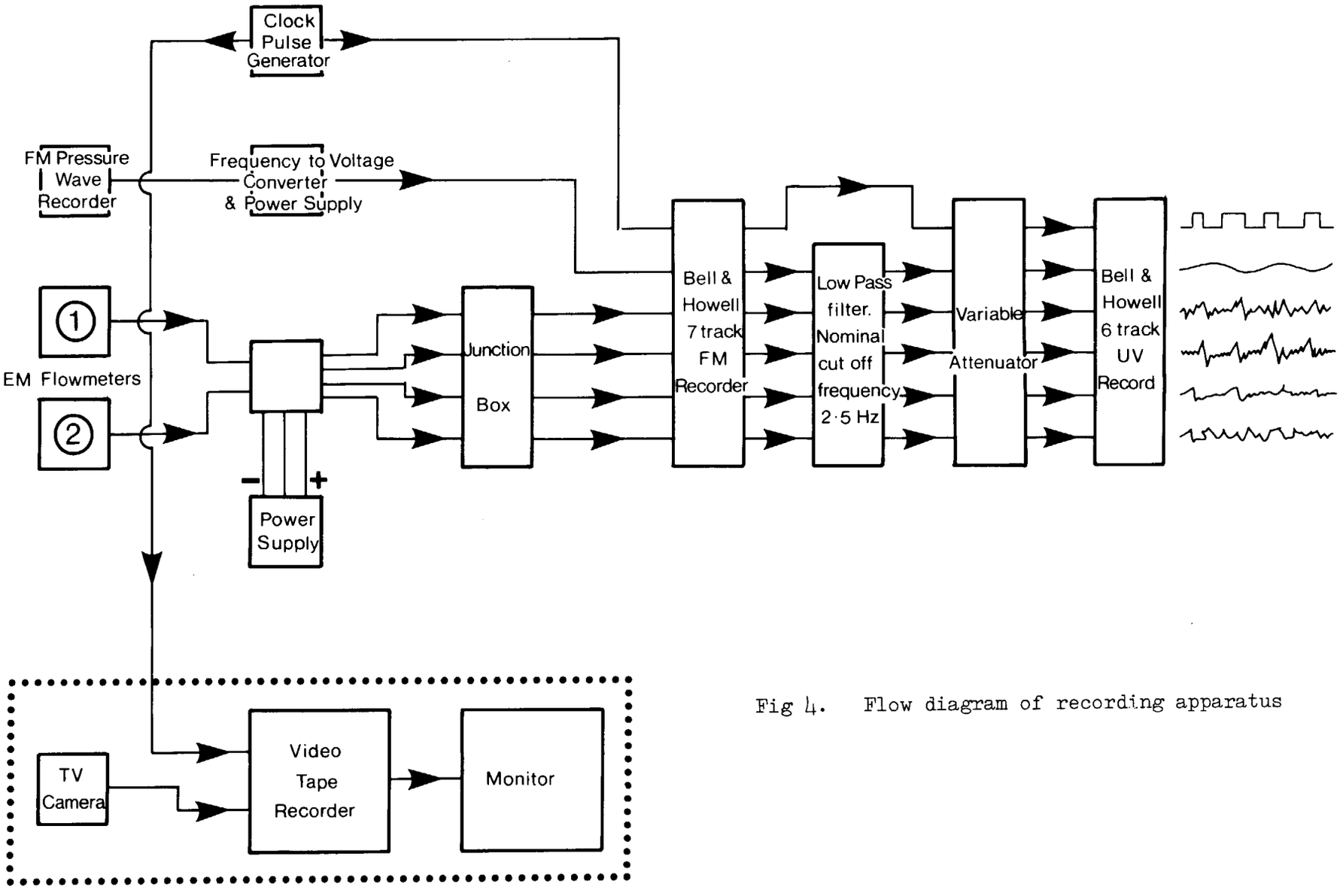

Fig 4. Flow diagram of recording apparatus

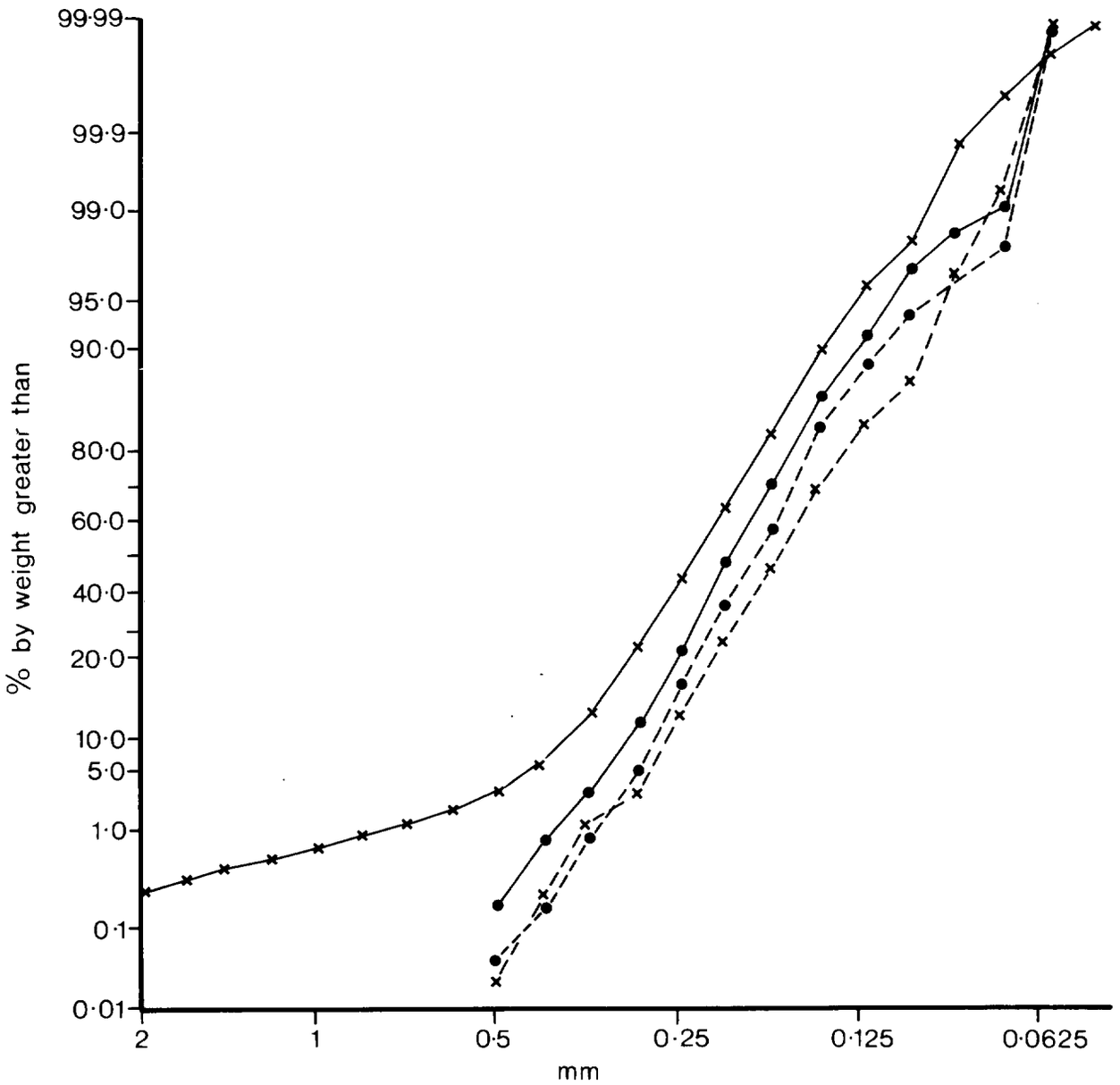

Fig 5. Cumulative grain size distribution.

× Indigenous sand (- - - - limits as tracer
(——— entire sand size fraction

• Tracer (- - - - red
(——— blue

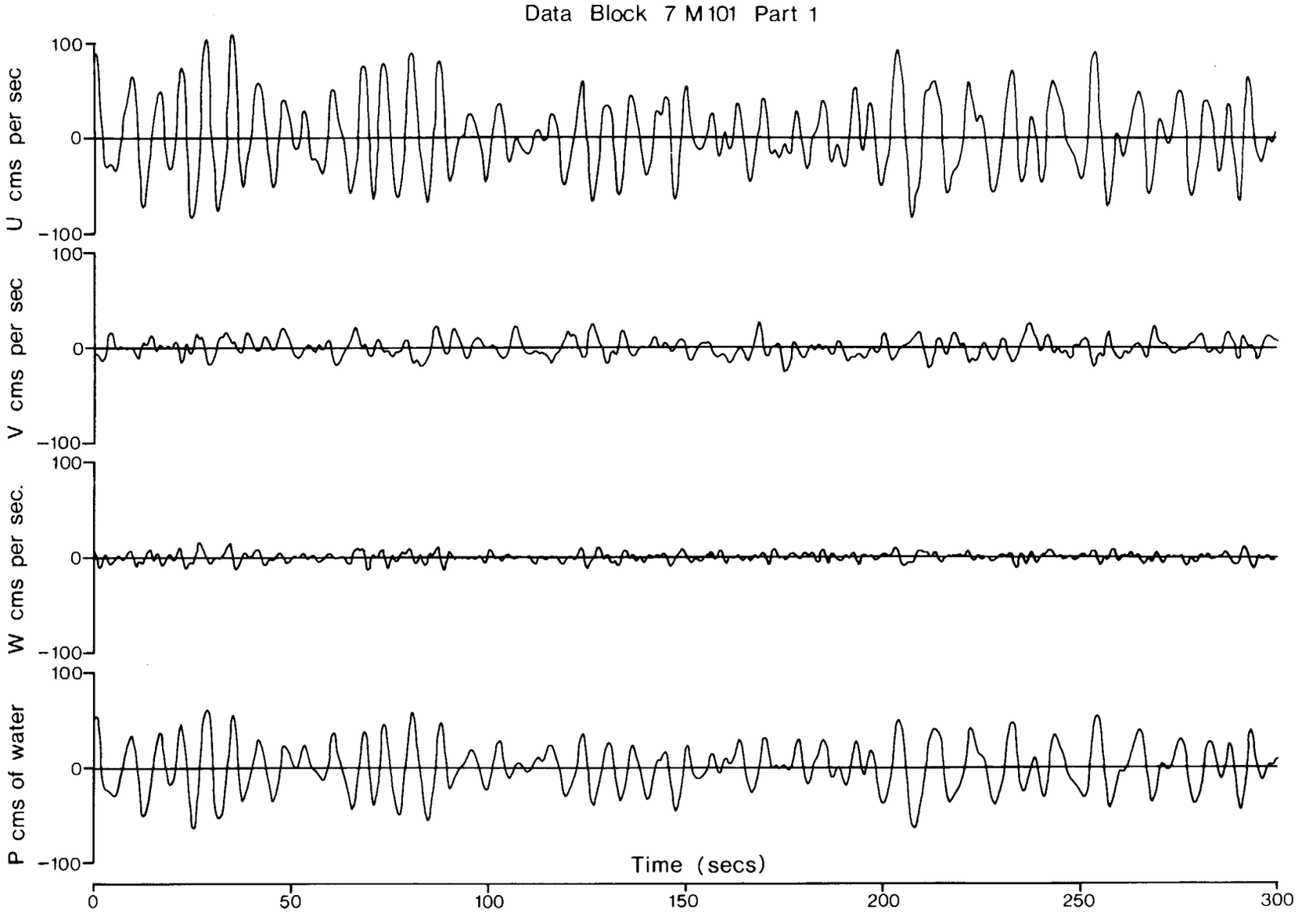

Fig 6. Typical time series plots

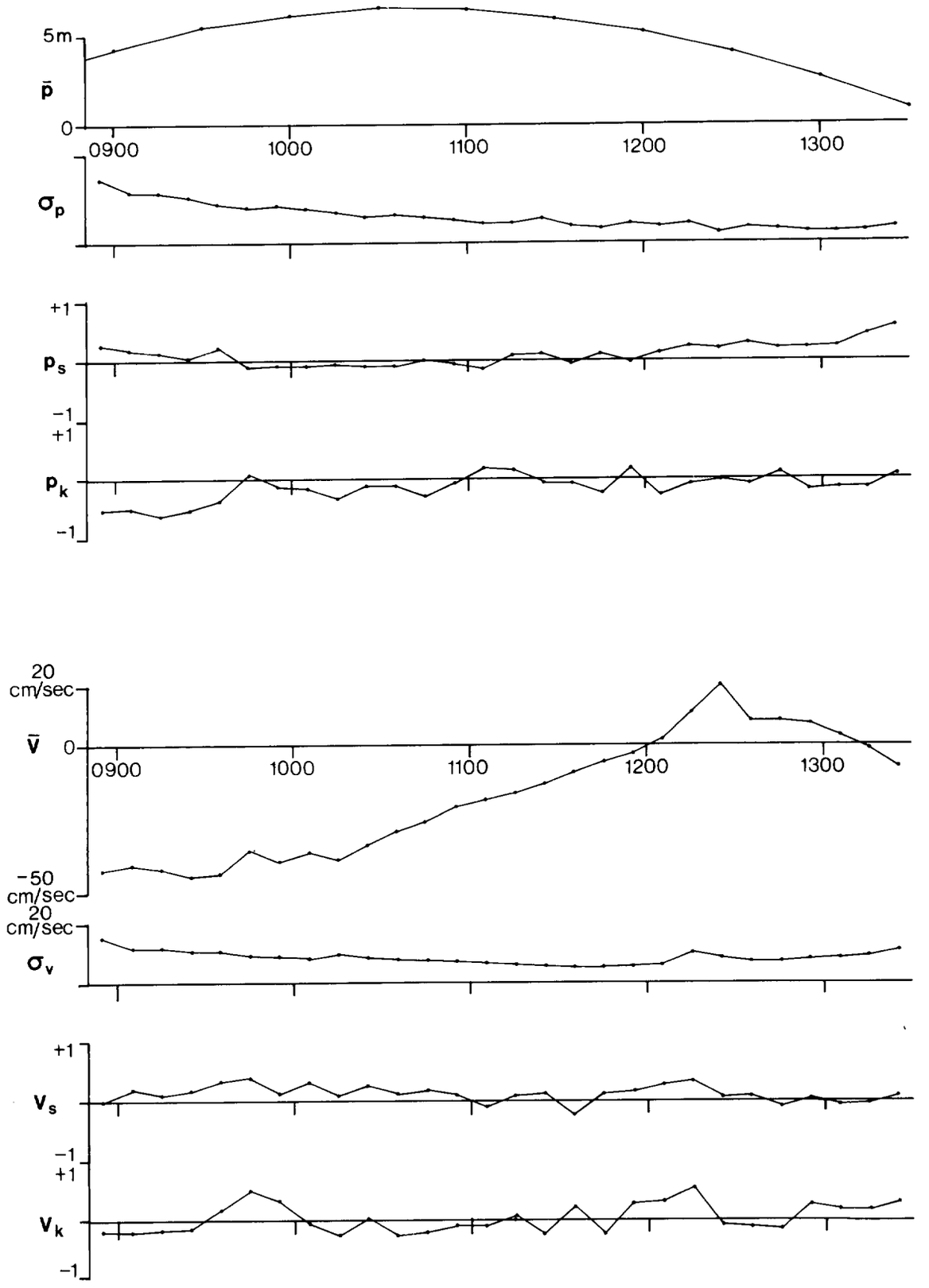

Fig 7a. Typical amplitude characteristics of pressure (**p**) and longshore velocity (**v**).

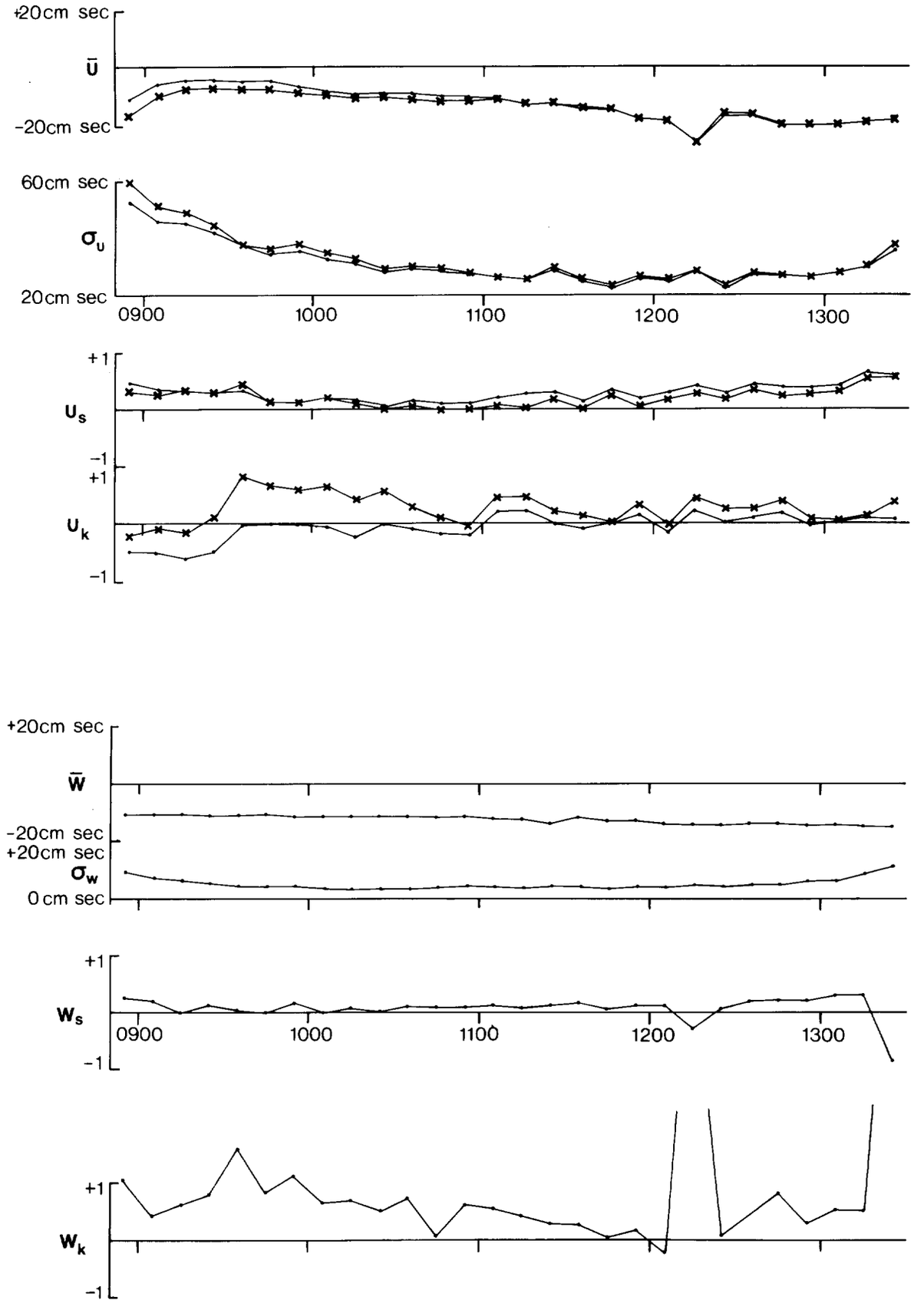

Fig 7b. Typical amplitude characteristics of onshore(**U**) and vertical (**W**) velocities.

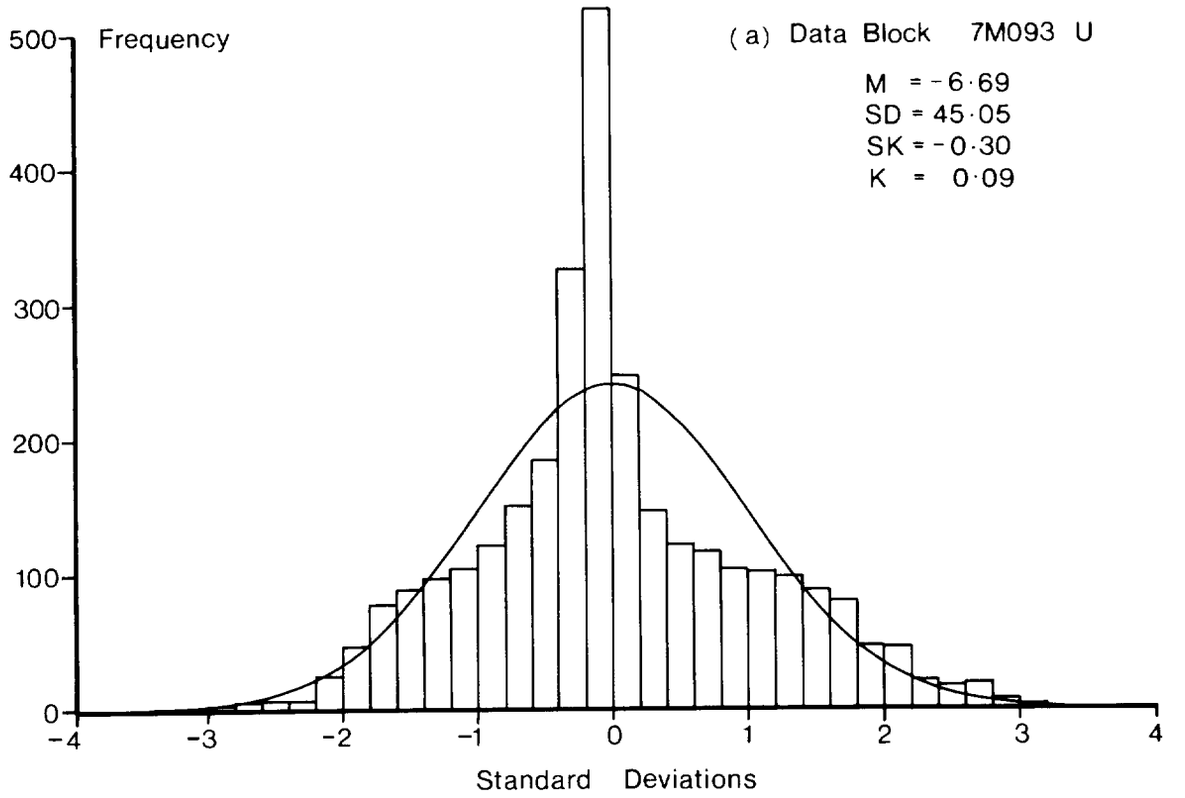

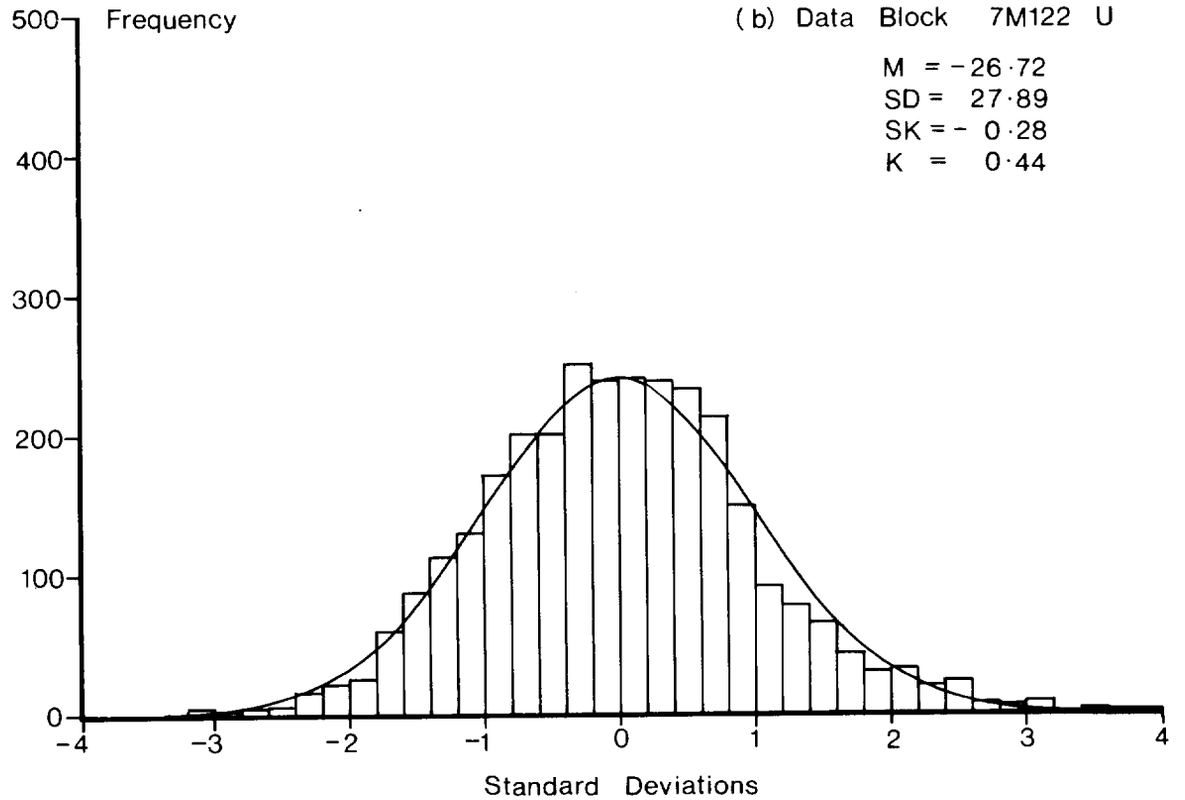

Fig 8. Examples of probability density function of onshore velocity.

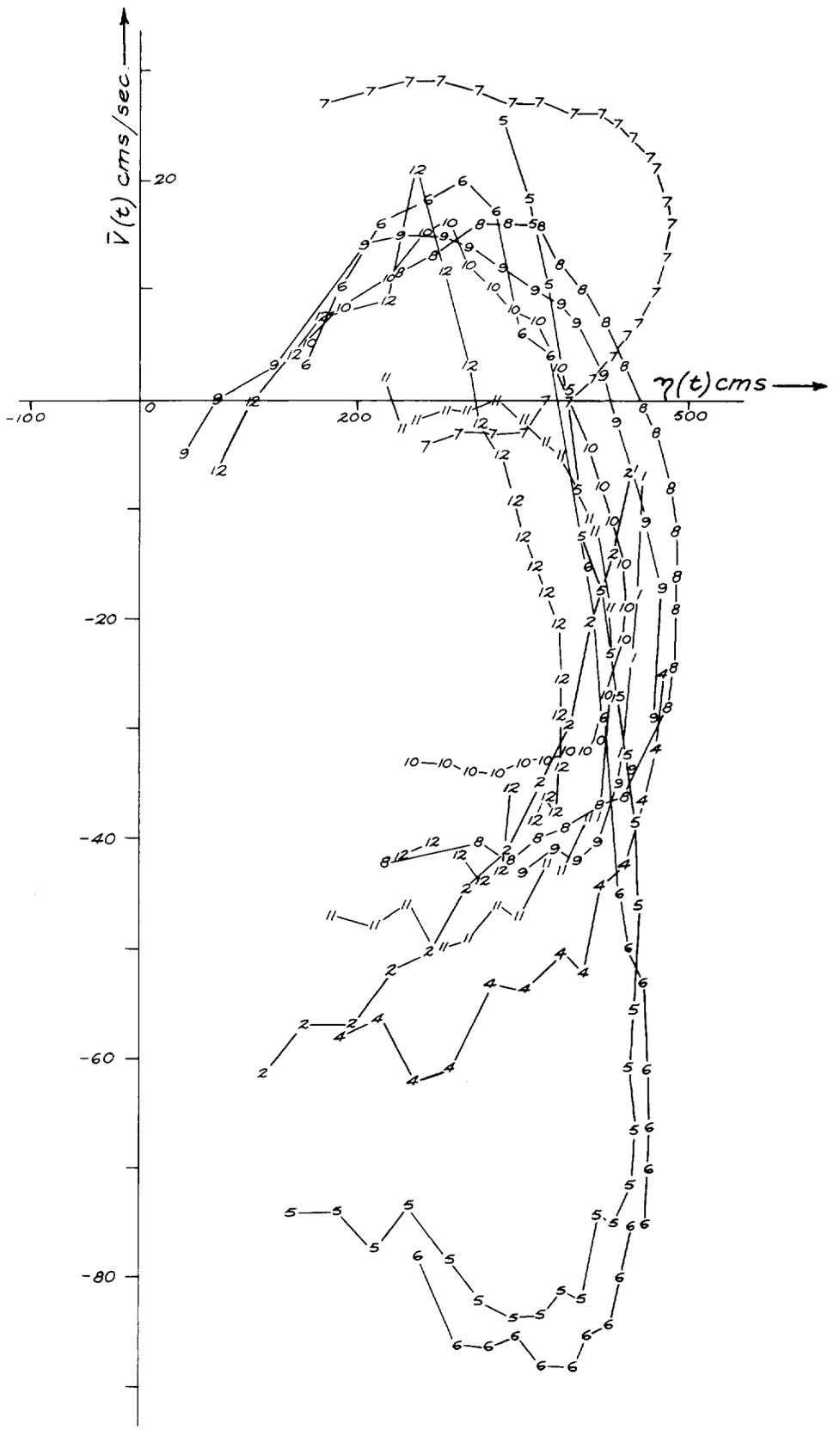

Fig 9 Surface elevation (η) against longshore velocity ($\bar{V}$)

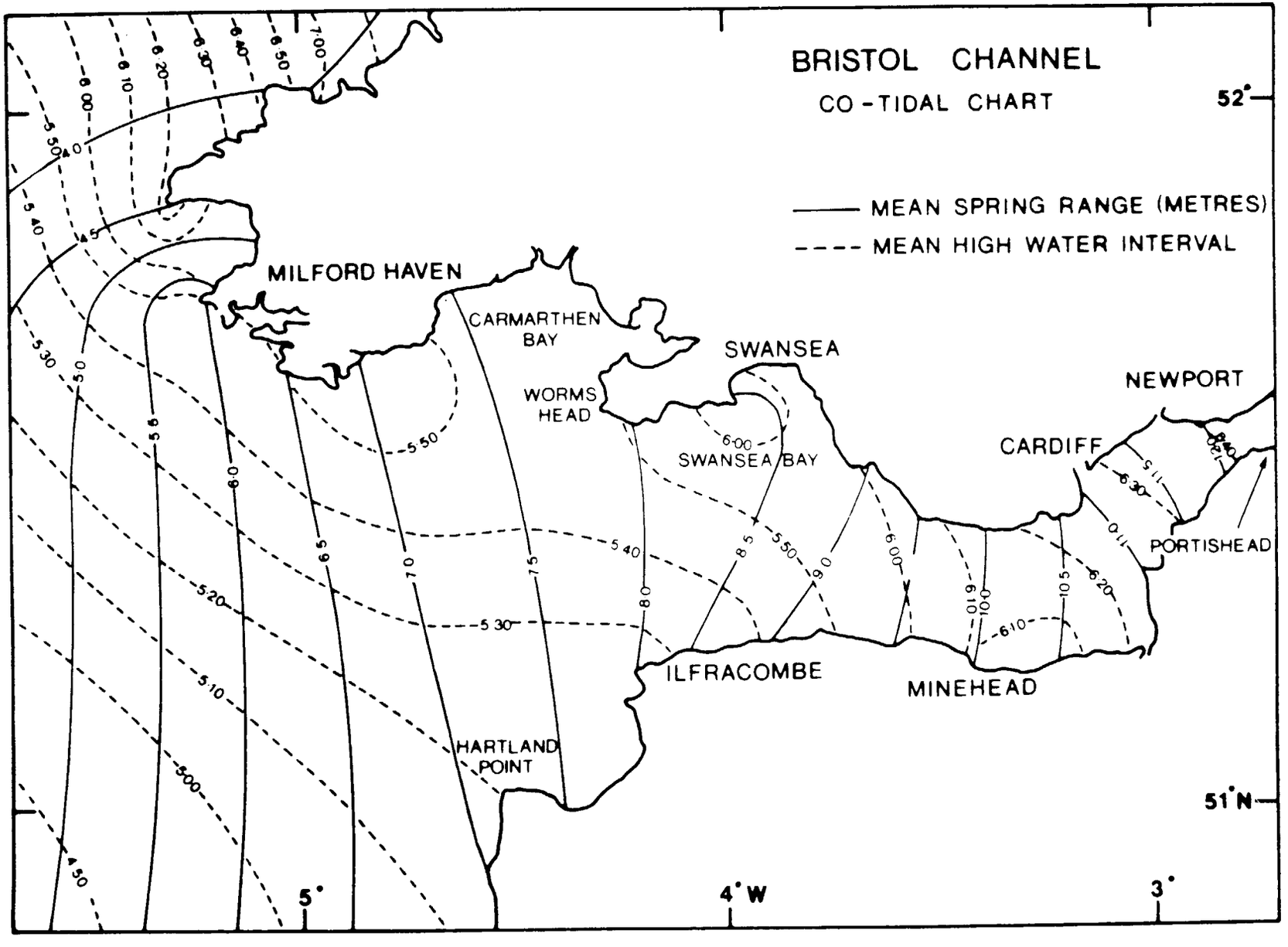

Fig 10. From Heathershaw and Hammond (1980)

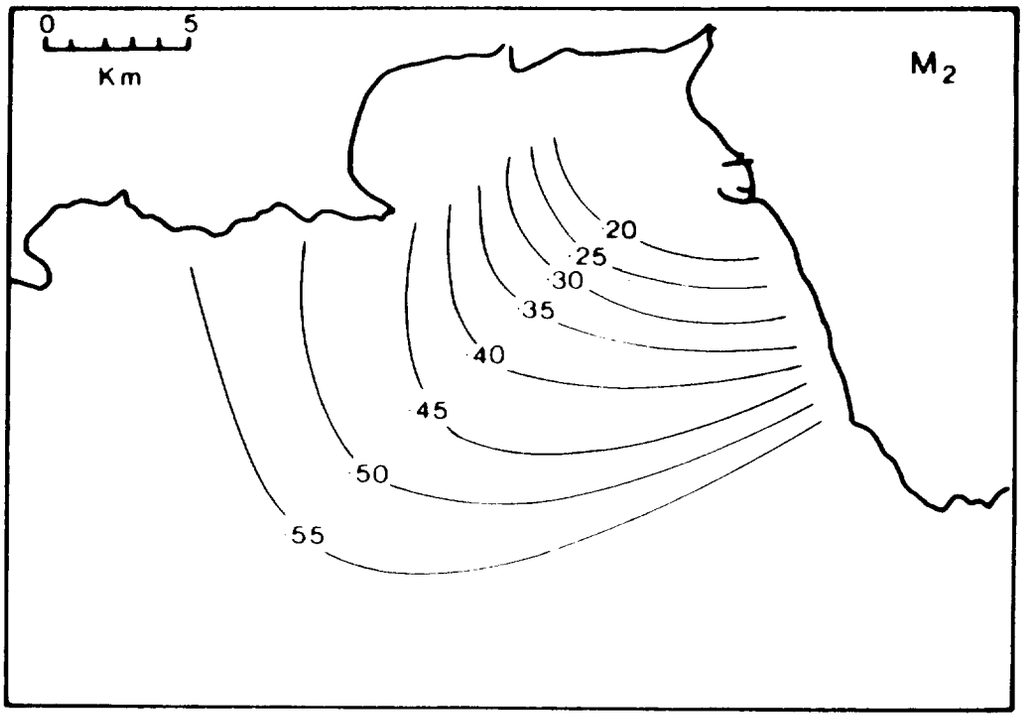

(a)

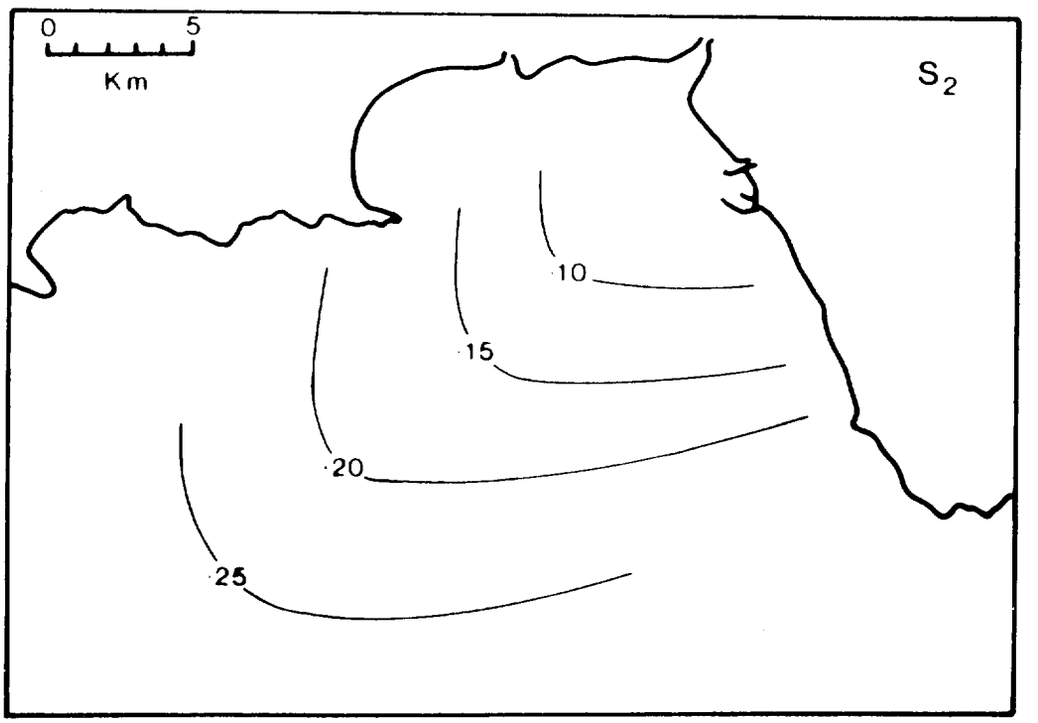

(b)

Fig 11. Amplitude of tidal constituents, from Heathershaw and Hammond (1980).

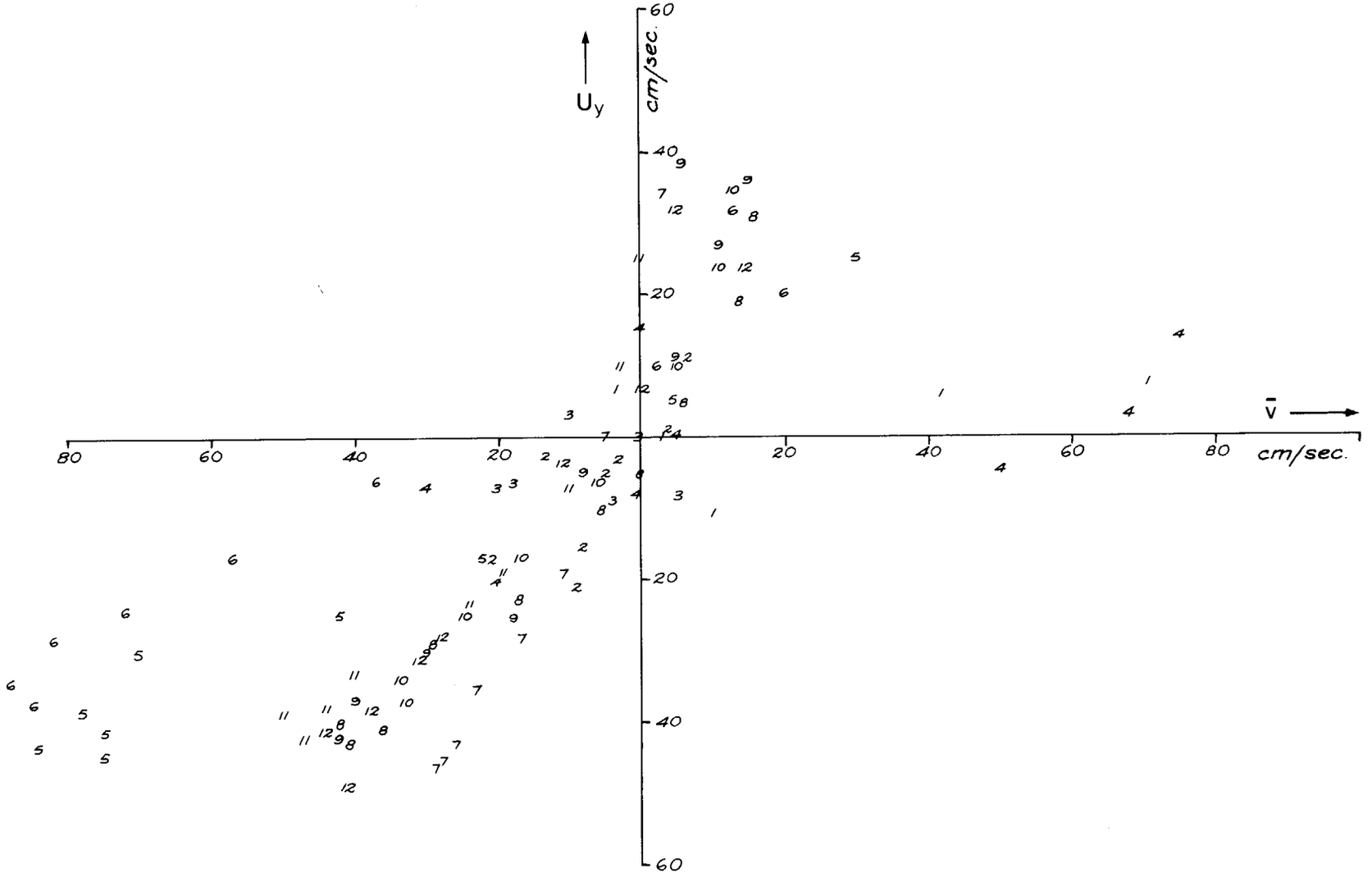

Fig 12. Comparison of longshore current on beach face ($\bar{V}$) with that measured offshore (U_y).

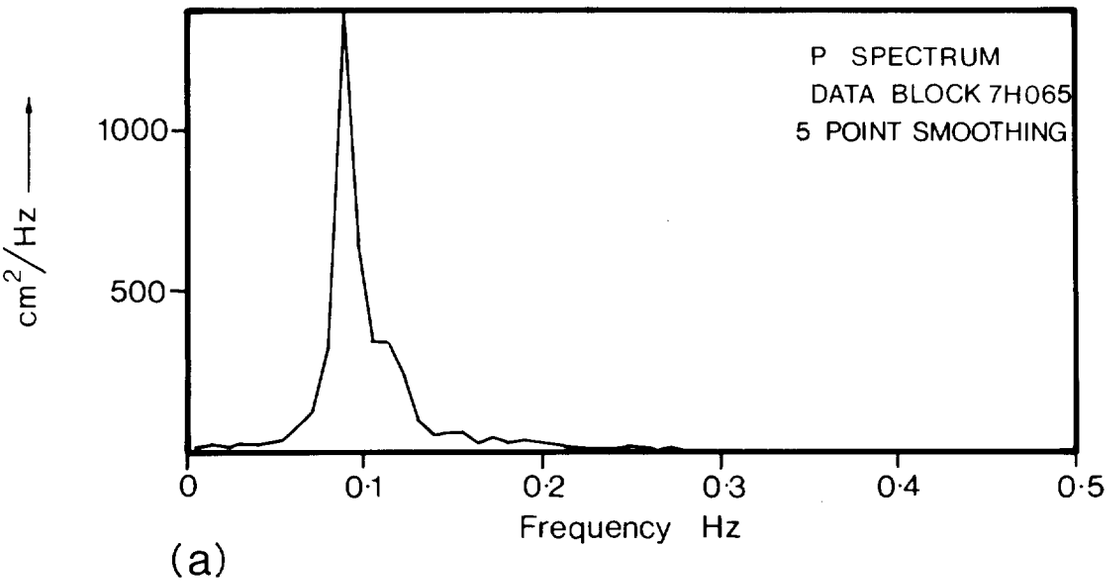

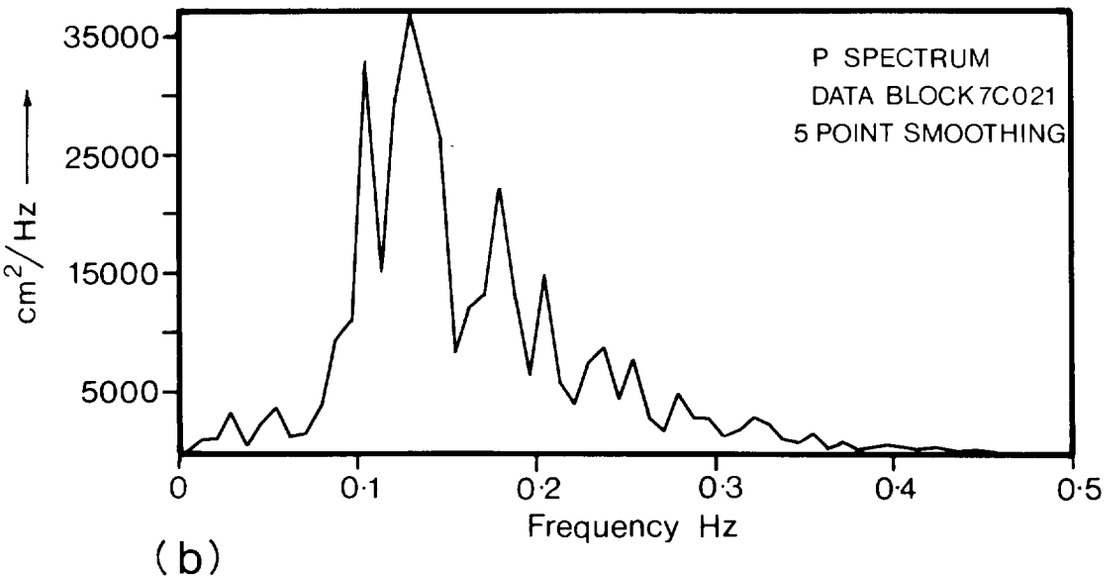

Fig 13. Typical pressure spectra

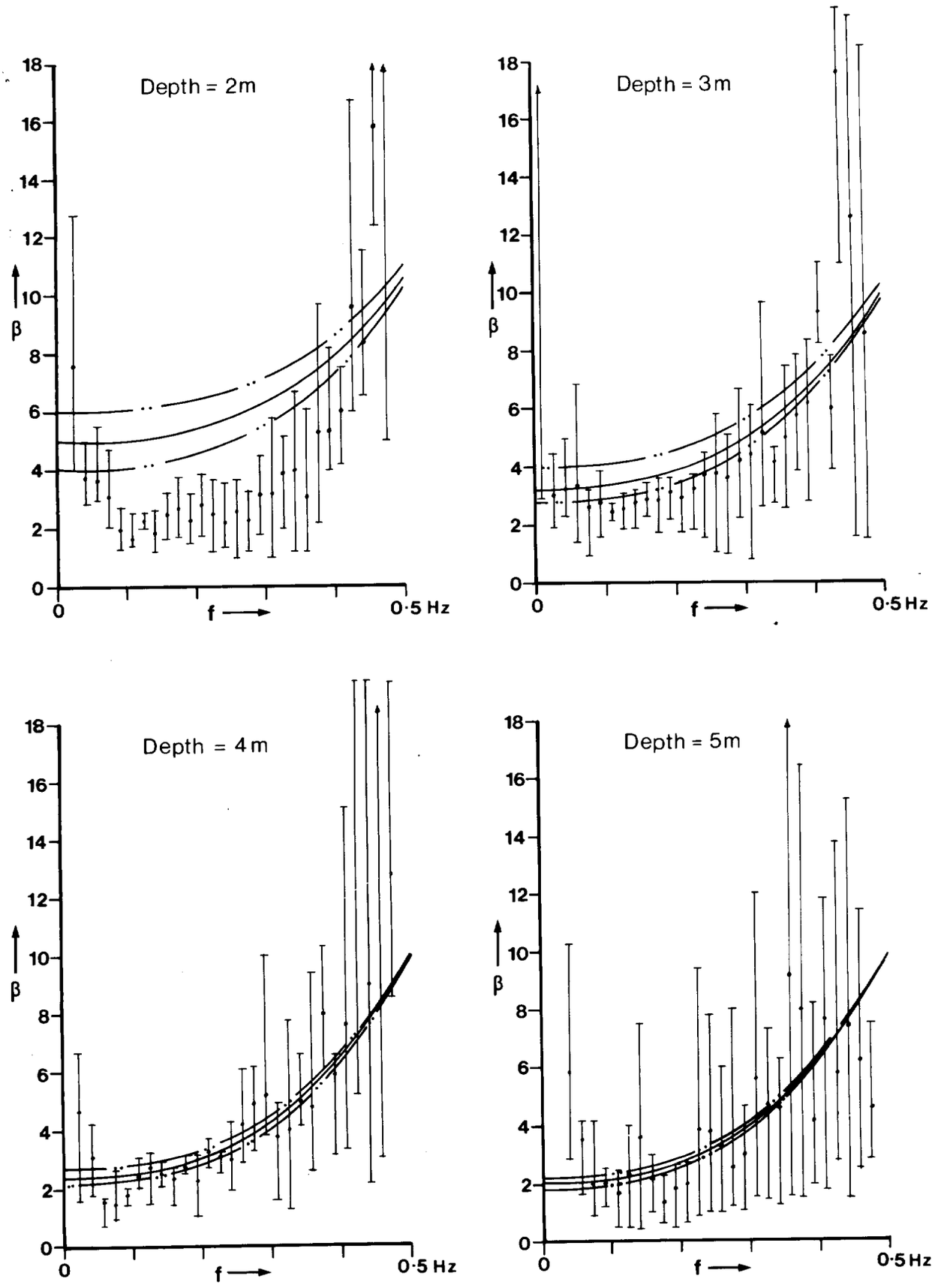

Fig 14. The ratio β ; the curves are theoretically derived

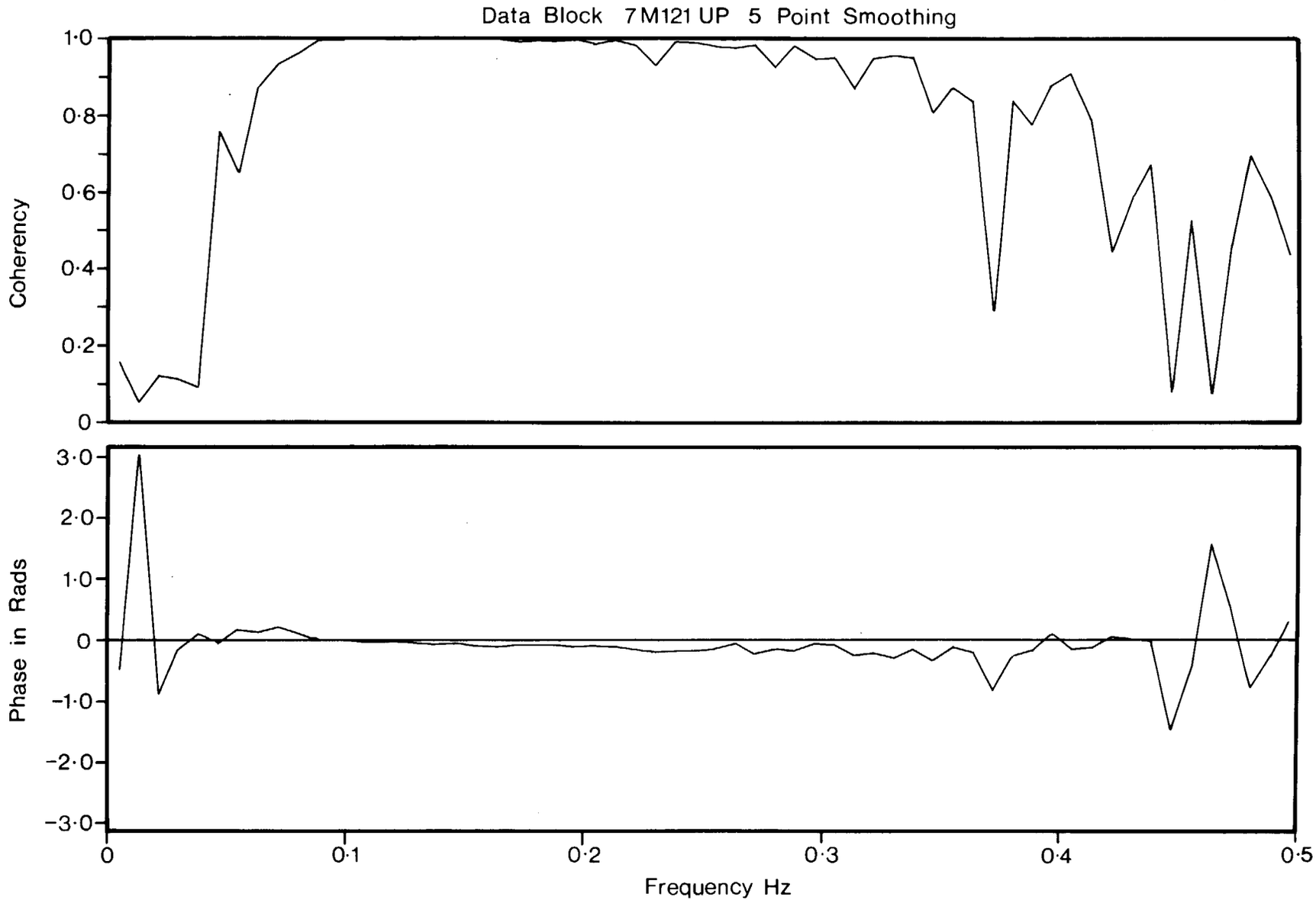

Fig 15. Example of phase and coherency between onshore velocity (**U**) and pressure (**p**).

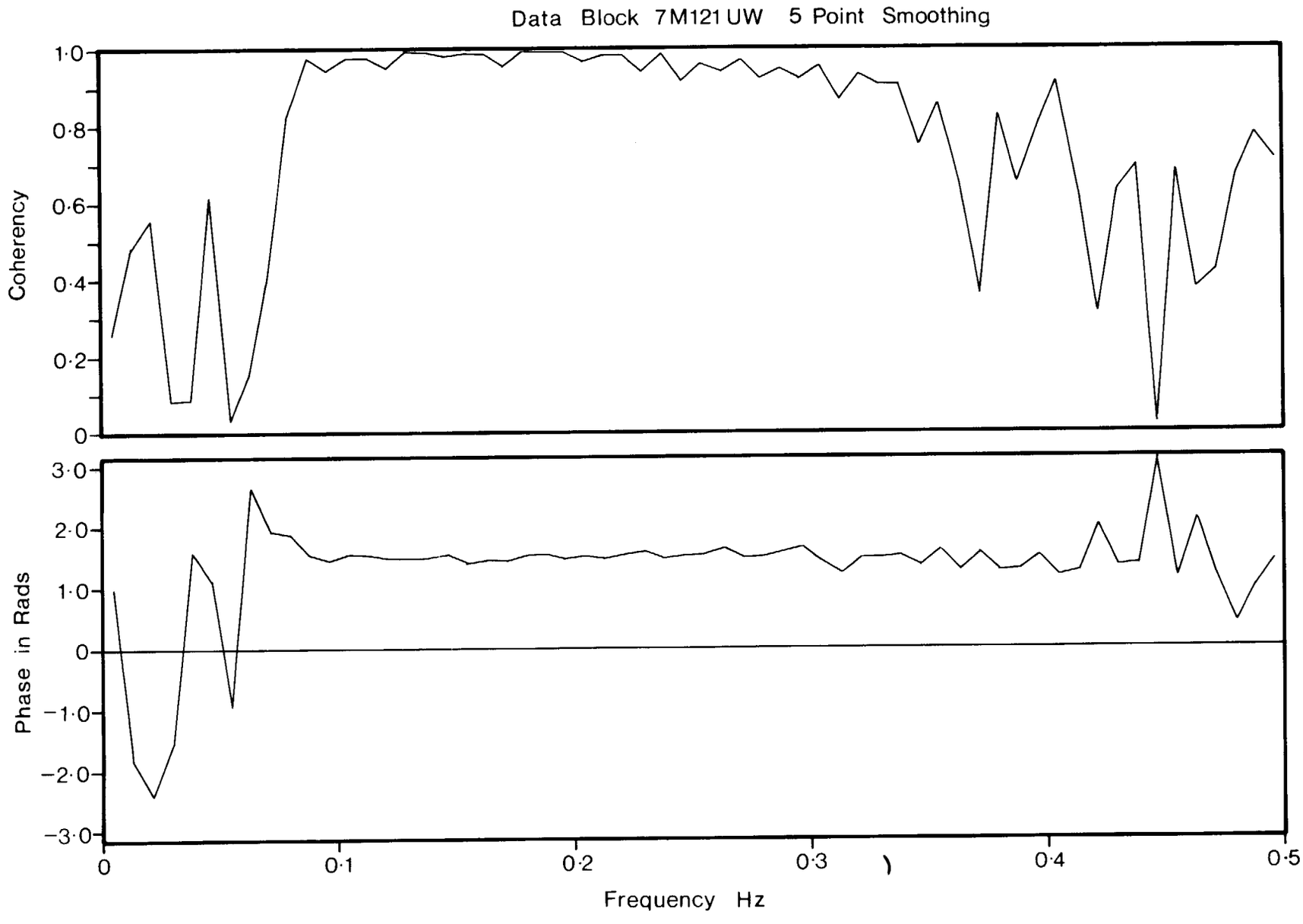

Fig 16. Example of phase and coherency between onshore (**u**) and vertical (**ω**) velocities

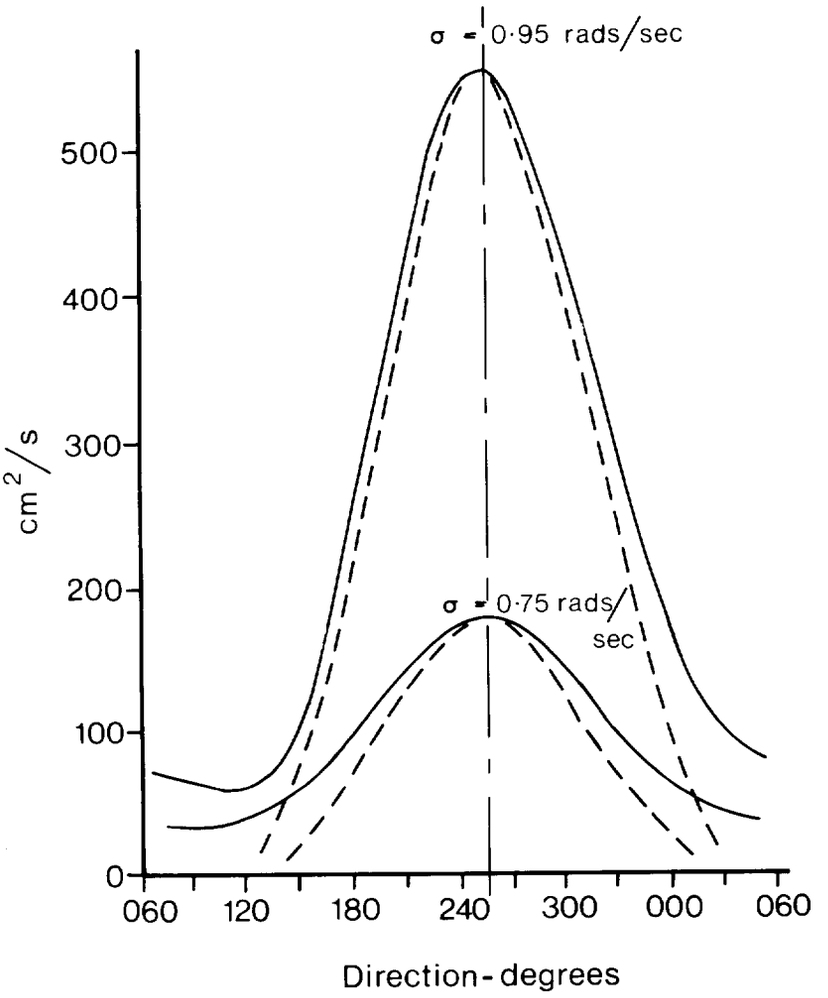

Fig 17. Comparison of observed directional spectra with that from a theoretical line spectra of zero width.
——— observed — — — — theoretical (from Bowden & White (1966))

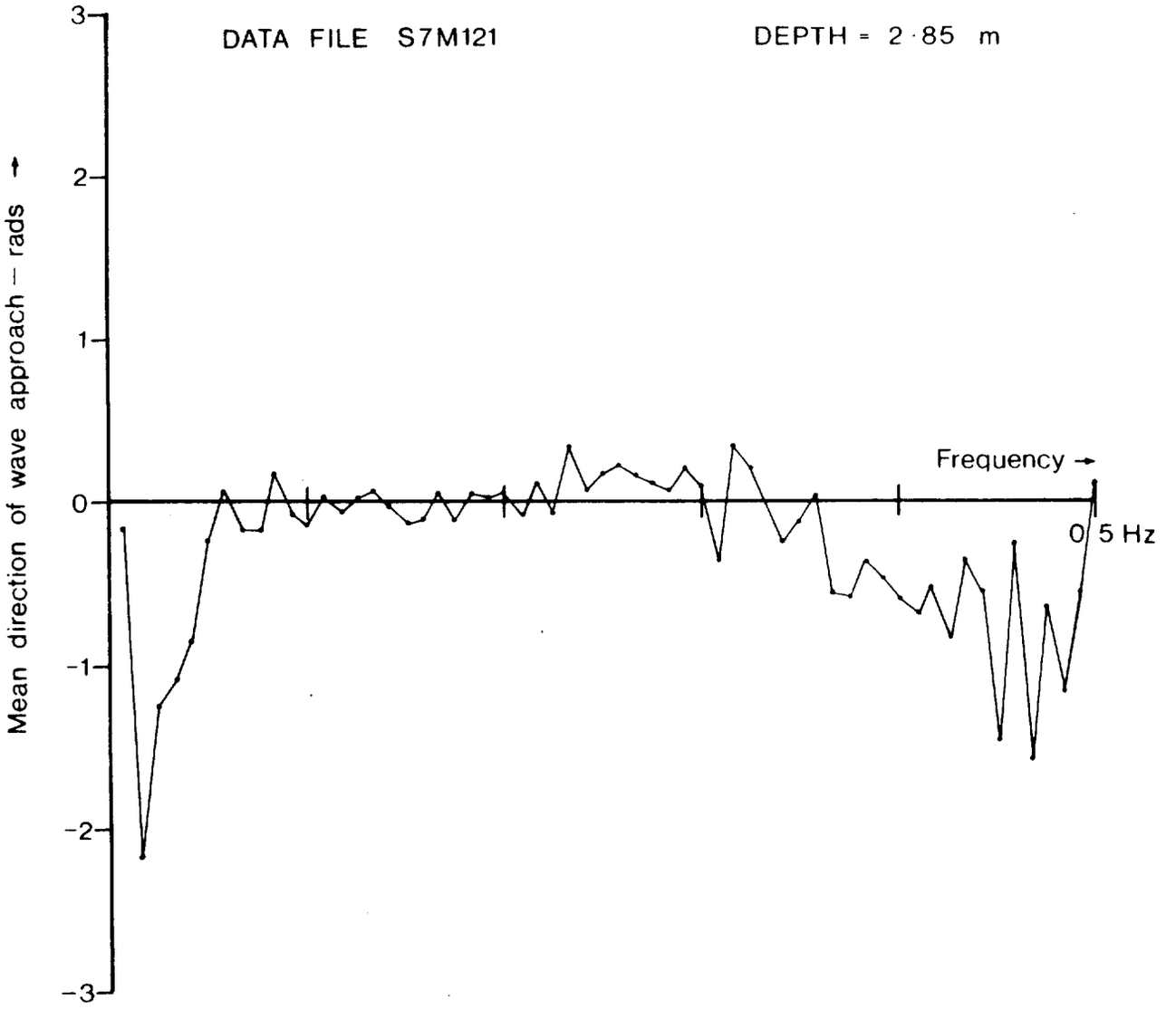

Fig 18. Typical mean direction spectrum

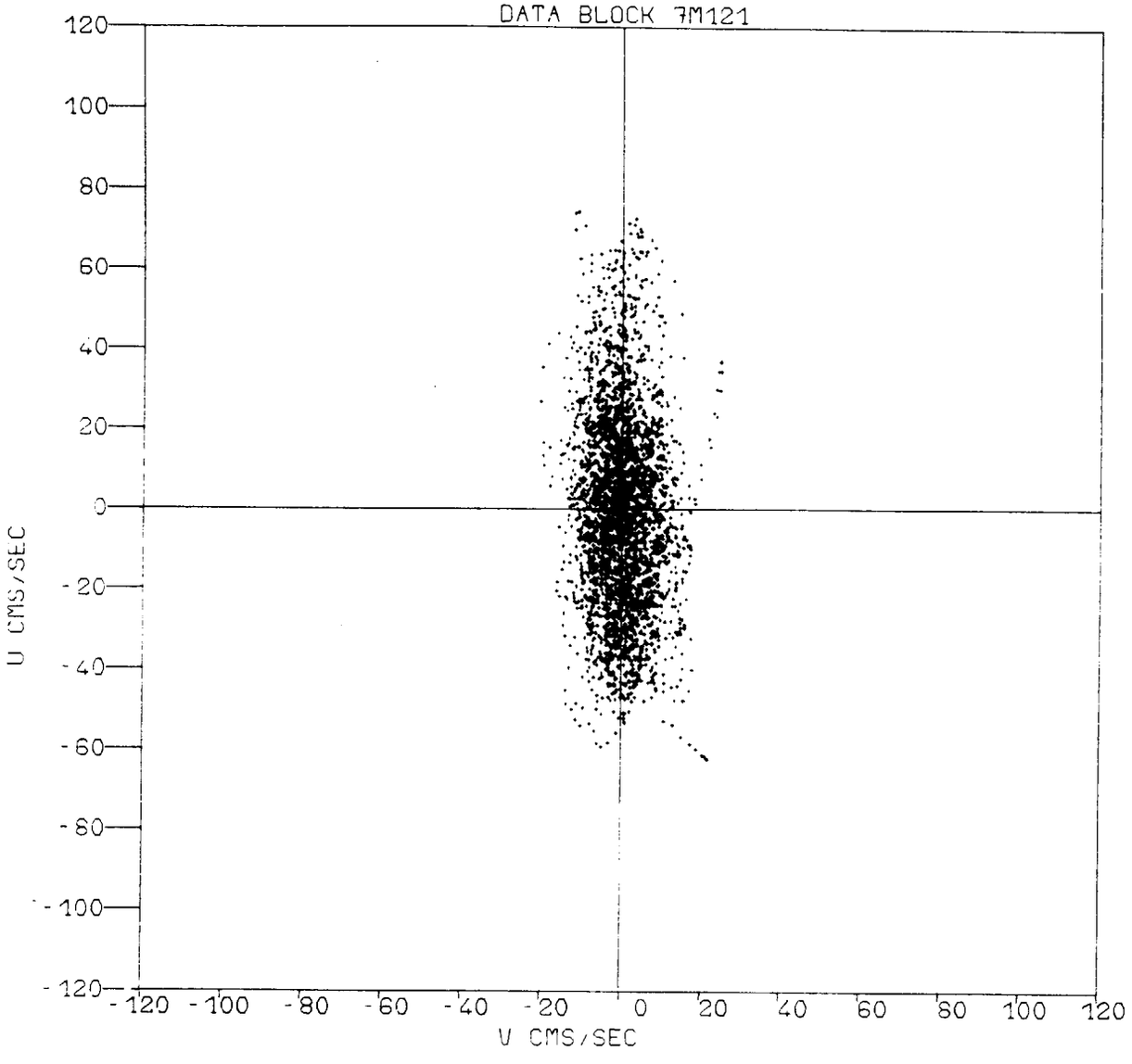

Fig 19. Typical **U-V** scatter plot

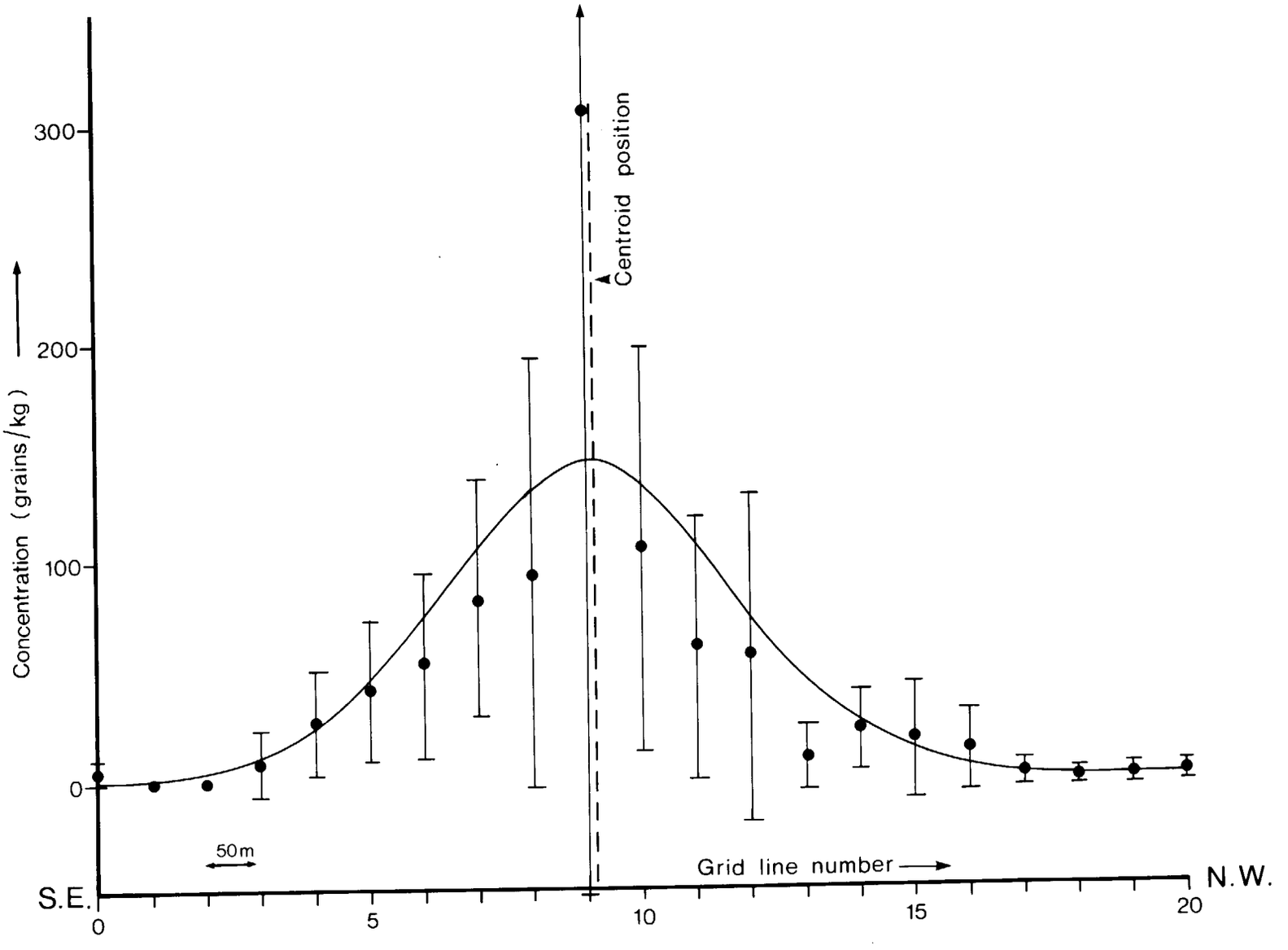

Fig 20. Longshore distribution of tracer remaining on beach after 6 months.

results with scatter bars

Gaussian distribution of similar mean and radius of gyration

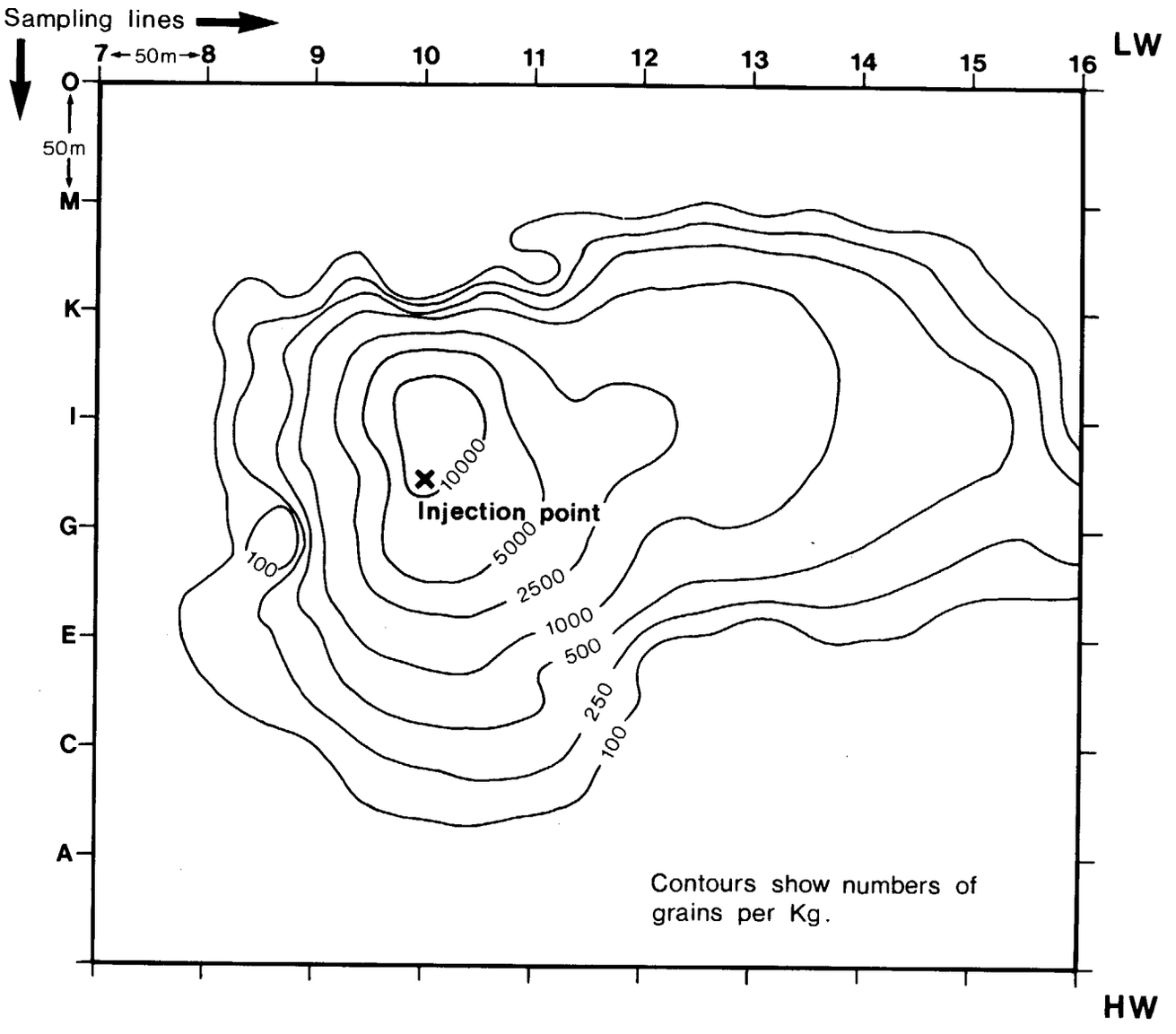

Fig 21. Examples of fluorescent tracer dispersal pattern; after 3 tides, 15 November 1976 (pm).

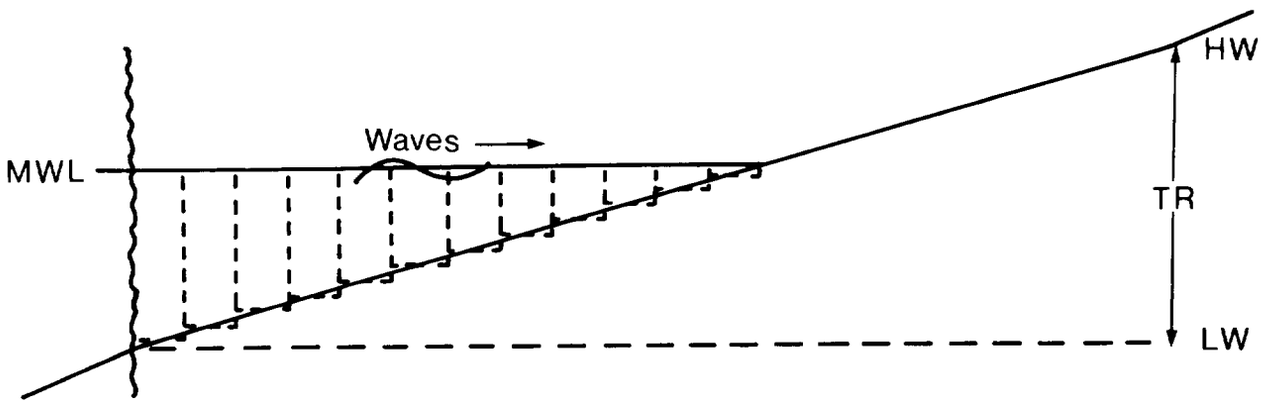

(a)

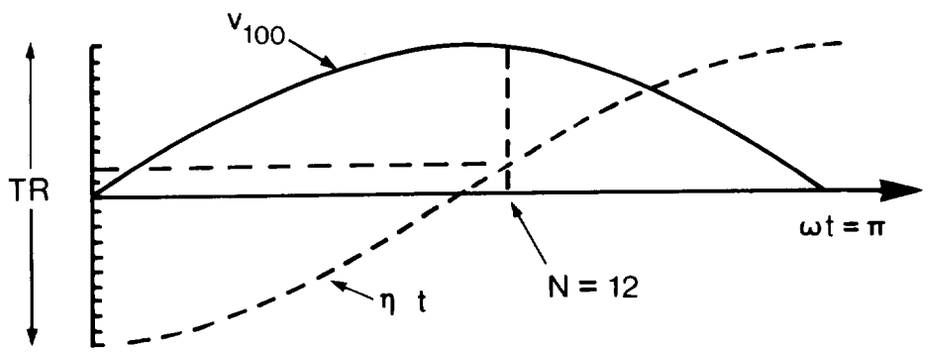

(b)

Fig 22(a) Cross section of beach for tidal transport calculations.

(b) Idealized behaviour of longshore tidal current (v_{100}) and surface elevation (η).

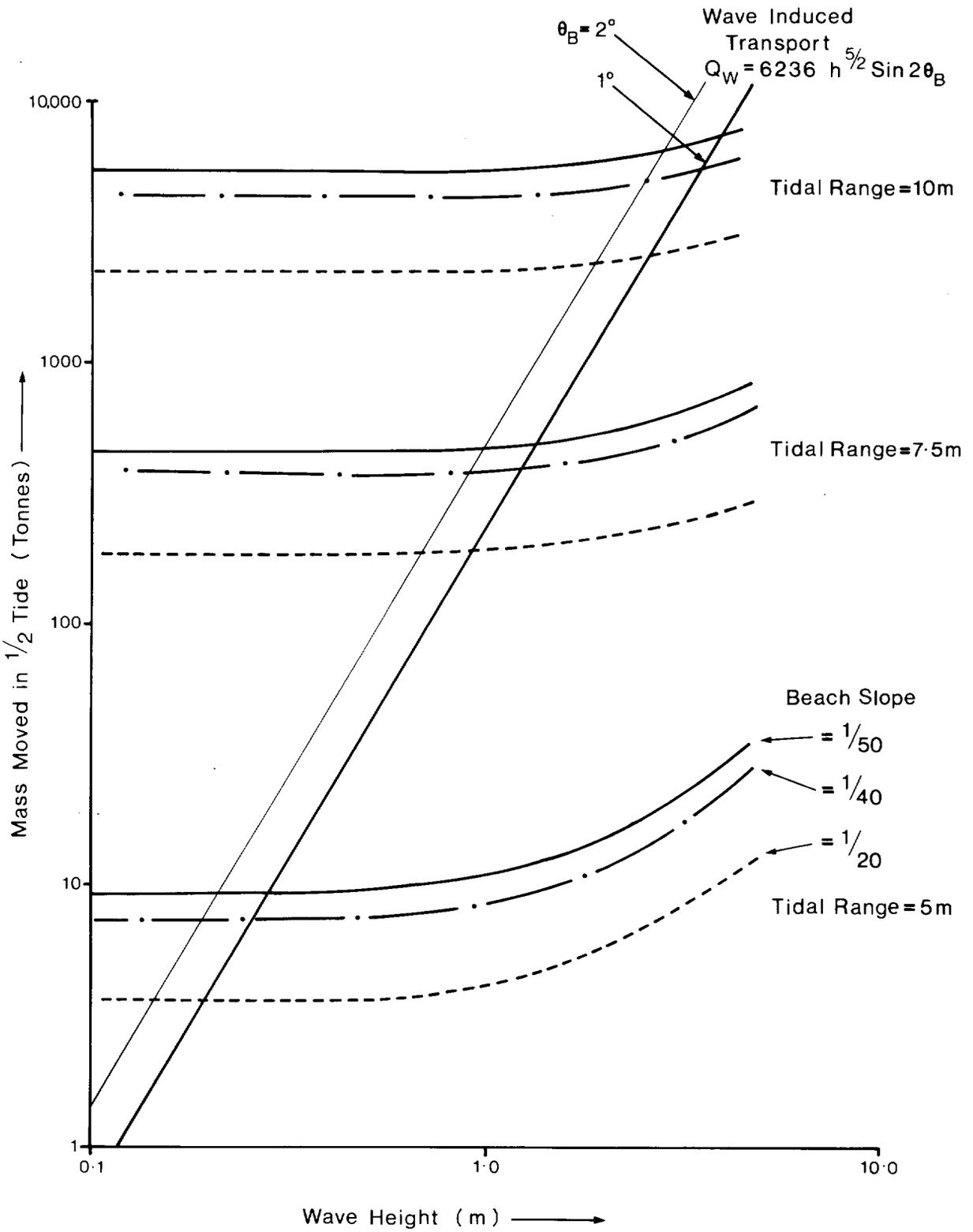

Fig 23. Relative competence of wave-induced and tidal longshore currents.

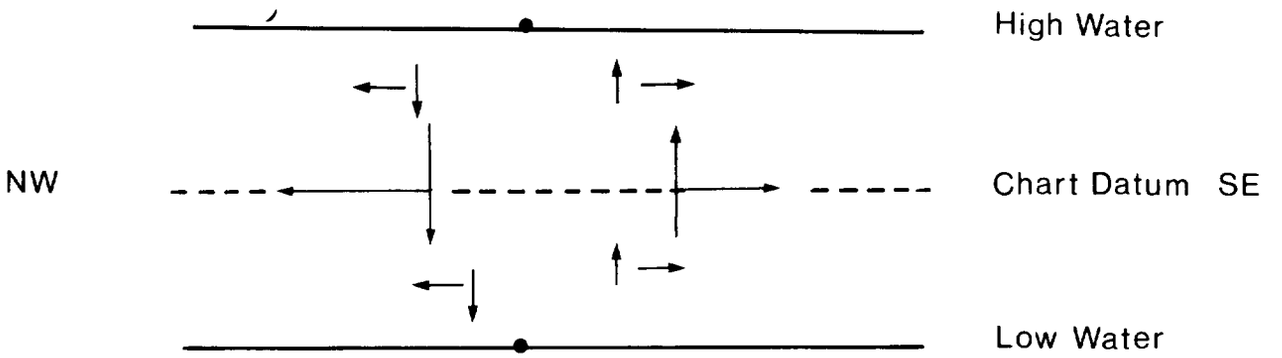

(a) Standing Tidal Wave

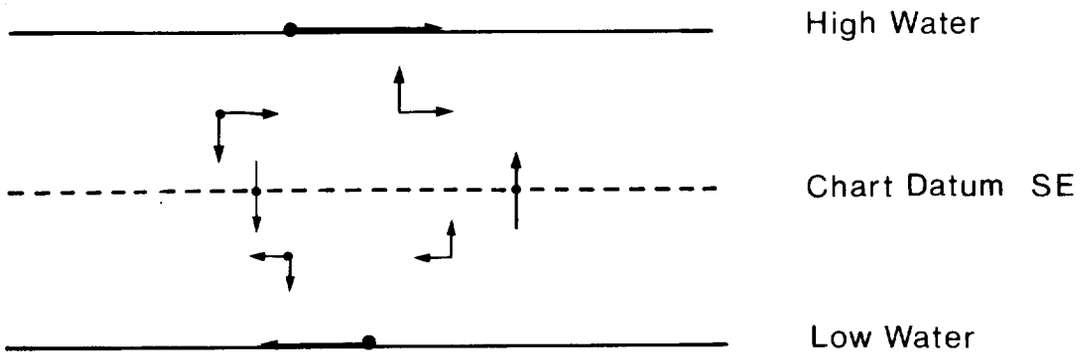

(b) Progressive Tidal Wave

Fig 24. Action of tidal wave on beach face in relation to water level.

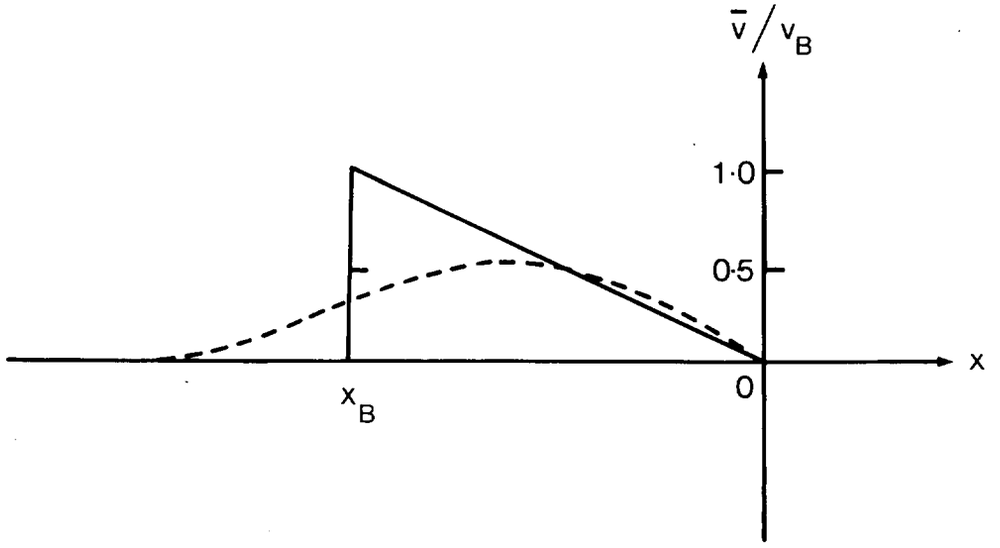

Fig 25. Theoretical wave-induced longshore current profile (from Longuet-Higgins (1972)).